OPTICAL COHERENCE TOMOGRAPHY FOR EARLY DETECTION OF DENTAL DISEASES: *IN VITRO* AND *IN VIVO* FEASIBILITY STUDIES

By

CHRISTINE CHARLES SAHYOUN

A thesis submitted to the

Graduate School-New Brunswick

and

The Graduate School of Biomedical Sciences

Rutgers, The State University of New Jersey

In partial fulfillment of the requirements

For the degree of

Master of Science

Graduate Program in Biomedical Engineering

Written under the direction of

Mark C. Pierce, Ph.D.

And approved by

_____

_____

_____

_____

New Brunswick, New Jersey

May, 2016

ABSTRACT OF THE THESIS

Optical coherence tomography for early detection of dental diseases: *in vitro* and *in vivo* feasibility studies

by **CHRISTINE CHARLES SAHYOUN**

Thesis Director:
Mark C. Pierce, Ph.D.

Inflammation of the gums and tooth decay are conditions that, if detected early enough, can be corrected or reversed. There is therefore a need for minimally invasive, accurate assessment of dental and periodontal tissue in order to achieve prompt diagnosis and treatment. Optical coherence tomography (OCT) is an emerging non-invasive, non-ionizing imaging modality that provides cross-sectional images of tissue, up to several millimeters in depth with micrometer level resolution. The underlying hypothesis of this thesis is that biological alterations to oral tissues result in changes in light scattering behavior which could be quantified by OCT.

In vitro bovine tooth samples were demineralized in 30% H_3PO_4 for exposure times ranging from 0 to 5 seconds. Volume OCT scans were taken and the mean backscattered intensity as a function of depth was generated for each exposure time. Microhardness indentation measurements were also recorded. A significant negative correlation ($p < 0.05$) was found between OCT surface peak intensity (dB) and Knoop hardness number (KHN).

Ten human subjects underwent OCT imaging before and after dry brushing the gingiva to induce inflammation. Mean backscattered OCT intensity versus depth plots were generated from pre- and post-brushing images. The slope of a linear fit to the intensity vs depth plot, and the area under the curve (AUC) were determined for epithelium and the lamina propria layers and compared between baseline and post-treatment. No appreciable factor change in either the fitted slope or AUC were measured for the epithelium ($p > 0.05$) and no appreciable factor change in the AUC was measured for the lamina propria ($p > 0.05$). There was a significant factor change in slope for the lamina propria region ($p < 0.05$).

The *in vitro* demineralization study established a relationship between OCT signal intensity and the current gold-standard of microhardness testing, suggesting that OCT may be able to quantify demineralization *in vivo*. The *in vivo* gingival study led to the development of the necessary protocols and software to perform measurements in future studies. Together, these studies provide support for further development of OCT as a diagnostic tool for the *in vivo* assessment of dental diseases.

ACKNOWLEDGEMENTS

First and foremost I want to thank Dr. Pierce for his support and guidance throughout this entire process. He is an incredible advisor and mentor, and has greatly encouraged my growth as a researcher. I also want to thank Dr. Hacihaliloglu, Dr. Silver, and Dr. Boustany for their willingness to be a part of my thesis and for helping me reach my goal with their knowledge and input.

A special thank you to Roger Ellwood, Deborah Peru, Robert Cantore and the whole team at Colgate-Palmolive for their guidance and mentorship during the course of my research endeavors. Their consultation was invaluable and the training and use of the facility's instrumentation was crucial for the success of my thesis.

Last, but certainly not least, I want to give a big thank you to my family and friends for their unending support and motivation. This is a reality because of all of you, and I am so thankful.

TABLE OF CONTENTS

LIST OF ACRONYMS

AUC – Area under the curve
CP-OCT – Cross-polarization optical coherence tomography
DEJ – Dentin-enamel junction
EP - Epithelium
FC – Factor change
GUI – Graphical user interface
KHN – Knoop hardness number
LP – Lamina propria
NIR – Near-infrared
OCT – Optical coherence tomography
ROI – Region-of-interest
SD-OCT – Spectral-domain optical coherence tomography
SS-OCT – Swept-source optical coherence tomography

LIST OF FIGURES

CHAPTER 1: INTRODUCTION

The overarching goal of this thesis is to evaluate the ability of optical coherence tomography (OCT) to provide noninvasive image-based assessment of oral tissues. This chapter begins with an overview of the importance of early detection of gum and tooth disease, some of the drawbacks of current clinical approaches for diagnosis, and how OCT might be utilized as a technique for assessing oral health. The principles of OCT are then introduced to demonstrate how this methodology works, and some of its current biomedical applications are discussed to demonstrate the clinical feasibility of OCT. Finally, research efforts in specifically imaging dental tissue with OCT are presented to provide the framework of and motivation behind this thesis.

1.1 MOTIVATION AND SIGNIFICANCE

With periodontal disease being linked to systemic issues such as cardiovascular disease, diabetes and pulmonary disease, proper oral hygiene and care is important for an individual's general health[1]. Gingivitis, a gum disease characterized by inflammation, and the more severe condition of periodontitis, which can result in damage and loss of the gums as well as tooth damage (**Figure 1a**), both serve as risk factors for systemic conditions, and the opposite has also been indicated with systemic disease negatively affecting the periodontium[1]. In addition to diseases of the gum, dental caries and decay (**Figure 1b**) can also have adverse effects on health specifically for children, affecting their growth and producing pain and inflammation[2]. Beyond physical well-being, oral health is important for an individual's quality of life both psychologically and socially[1].

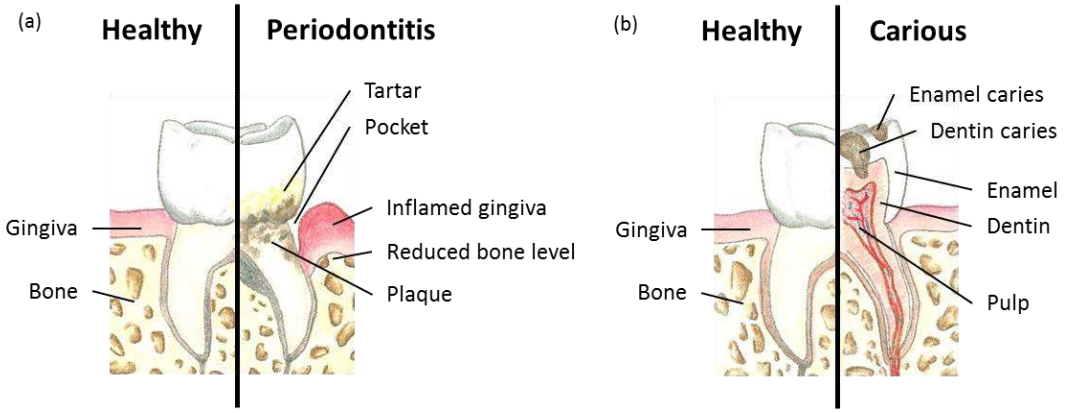

Figure 1 – **(a)** An illustration depicting the key differences between healthy periodontium and one with periodontitis. With periodontitis, the gingiva is inflamed pulls away from the teeth forming a pocket, and the bone level goes down. **(b)** An illustration depicting the key differences between a healthy tooth and one with caries.

If realized early in the process, some of these issues can be corrected or even reversed, making it important to have reliable methods of detection. For periodontal diseases several different parameters are assessed through physical examination, including probing pocket depths, probe-induced bleeding, clinical attachment loss, and more recently measurement of salivary markers[3,4]. The current standard for detecting problems within the hard tissue (enamel and dentin) is radiography. While cracks and caries can be identified with this methodology, often times these lesions can only be detected through radiography once the disease has progressed significantly[5]. There is a need for a less invasive and more accurate and quantitative assessment of both dental and periodontal tissue to allow for prompt diagnosis and subsequent treatment. Optical coherence tomography (OCT) may be the solution.

OCT is an imaging modality that provides high-resolution cross-sectional images of turbid media, which can be of particular interest in biomedical applications. These images are generated by measuring the differences in backscattered light of sub-surface

tissue structures in response to a near-infrared (NIR) beam[6,7]. OCT is appealing in that it is noninvasive and provides real-time tissue assessment of < 15 μm resolution and 2 – 3 mm depths; these features are approaching histopathology, a general standard for pathological diagnoses[7]. OCT has been used in ophthalmic imaging since pivotal research conducted by Huang *et al.* in 1991, now allowing physicians to evaluate structural changes of the retina and diagnose various diseases including glaucoma, age-related macular degeneration, and macular edema[7]. Atherosclerotic plaques and various forms of cancer (cervical, esophageal, and colon) can be visualized and distinguished using OCT due to their differing optical scattering properties[7].

As enamel demineralizes, its microstructure and refractive index changes, creating OCT-detectable variations in backscattered intensity. In gingival tissue, physiological changes and inflammation may also lead to differences in backscattered light, providing a possible parameter to evaluate periodontal health. Since OCT uses non-ionizing optical radiation, it could potentially provide such diagnoses at an earlier time point, without harmful exposure and with greater sensitivity than radiography[5].

1.2 PRINCIPLES OF OCT

The principles of OCT are commonly compared to those of ultrasound. With ultrasound, a sound wave is transmitted into the tissue, and the backscattered sound wave will depend on the varying acoustic properties of the different structures within the tissue; the reflected waves have corresponding echo time delays and amplitudes from which the characteristics of the internal structures are determined[7]. With OCT, instead of using sound, NIR light is utilized and the refractive index mismatch between different structural

components result in detectable differences in backscattered light intensity[7]. Since the speed of light is 10^5 times greater than that of sound, it is not possible to directly measure the echo time delay, as is done in ultrasound[7]. Instead, low-coherence interferometry must be used to determine the echo time delay by comparing the light received from the sample to light reflected from a reference path of known length and time delay[7]. By altering the reference path length, a single "A-line" of the sample can be acquired[8], and in order to generate an image ("B-scan") many A-lines must be taken across the sample; both of these factors result in a slow acquisition time of a few frames per second[8,9].

To provide real-time imaging with reasonable resolution and acquisition rates in this "time-domain" approach requires complex mechanical and optical reference arm designs[10]. To overcome this, researchers began investigating a spectral discrimination approach termed "Fourier Domain OCT," where the interferometric signal is acquired as a function of optical wavenumber[8,10,11] This can be achieved in two ways: (1) by using a broadband light source with a spectrometer for detection ("spectral-domain OCT" or SD-OCT), or (2) by using a single photodiode detector with a wavelength-swept narrowband light source ("swept-source OCT" or SS-OCT)[9]. Either approach yields the interferometric signal as a function of optical wavenumber, $I(k)$. The backscattered intensity as a function of depth, $I(z)$, can be determined by taking the Fourier transform of $I(k)$[9,11], and therefore generate an A-line. By transverse scanning, many A-lines can be acquired to provide a final cross-sectional image.

To perform SD-OCT, a broadband light source and spectrometer must be used[9], as pictured in **Figure 2**. The beam splitter sends one beam to the reference mirror (R) and

the other beam over to the sample (*S*). The sample and reference arms are then assumed to be illuminated by electric fields[12] with amplitude *A* and phase *Φ*:

$$A_R = A_{R_0} e^{i(kZ_R + \Phi_R)}$$

$$A_S = A_{S_0} e^{i(kZ_S + \Phi_S)}$$

Where *k* is the wavenumber, which is equal to $2\pi/\lambda$. On returning to the beam splitter, these two fields then combine and interfere in the following way:

$$A_{Interference} = A_R + A_S$$

The intensity of the interference signal is calculated as:

$$I_{interference} = \left|A_{interference}\right|^2 = |A_R + A_S|^2$$

$$I_{interference} = |A_R + A_S|^2 = (A_R + A_S)(A_R + A_S)^* \quad * \textit{denotes complex numbers}$$

$$= A_R A_R^* + A_S A_S^* + A_R A_S^* + A_S A_R^*$$

$$= I_R + I_S + A_{R_0} A_{S_0} e^{i(kZ_R + \Phi_R)} e^{-i(kZ_S + \Phi_S)}$$

$$+ A_{R_0} A_{S_0} e^{-i(kZ_R + \Phi_R)} e^{i(kZ_S + \Phi_S)}$$

$$= I_R + I_S + A_{R_0} A_{S_0} \left[e^{i(kZ_R + \Phi_R - kZ_S - \Phi_S)} + e^{-i(kZ_R + \Phi_R - kZ_S - \Phi_S)}\right]$$

Remembering the following relationship:

$$\cos(\theta) = \frac{e^{i\theta} + e^{-i\theta}}{2}$$

We can then write the intensity equation as:

$$I_{interference}(k) = I_R + I_S + \sqrt{I_{R_0} I_{S_0}}\left[2\cos(kZ_R - kZ_S + \Phi_R - \Phi_S)\right]$$

$$= \underbrace{I_R + I_S}_{\text{DC Terms}} + \underbrace{2\sqrt{I_{R_0} I_{S_0}}[\cos(k\Delta Z + \delta\Phi)]}_{\text{Interference Term}}$$

After removing the DC components, by simply taking the Fourier Transform of the intensity as a function of *k*, the frequencies of the fringes can be obtained. If there was just one single reflector in the sample arm, the result would be similar to that seen in **Figure 2**, where there is a single peak representing the intensity at that particular depth – or one point on an A-line.

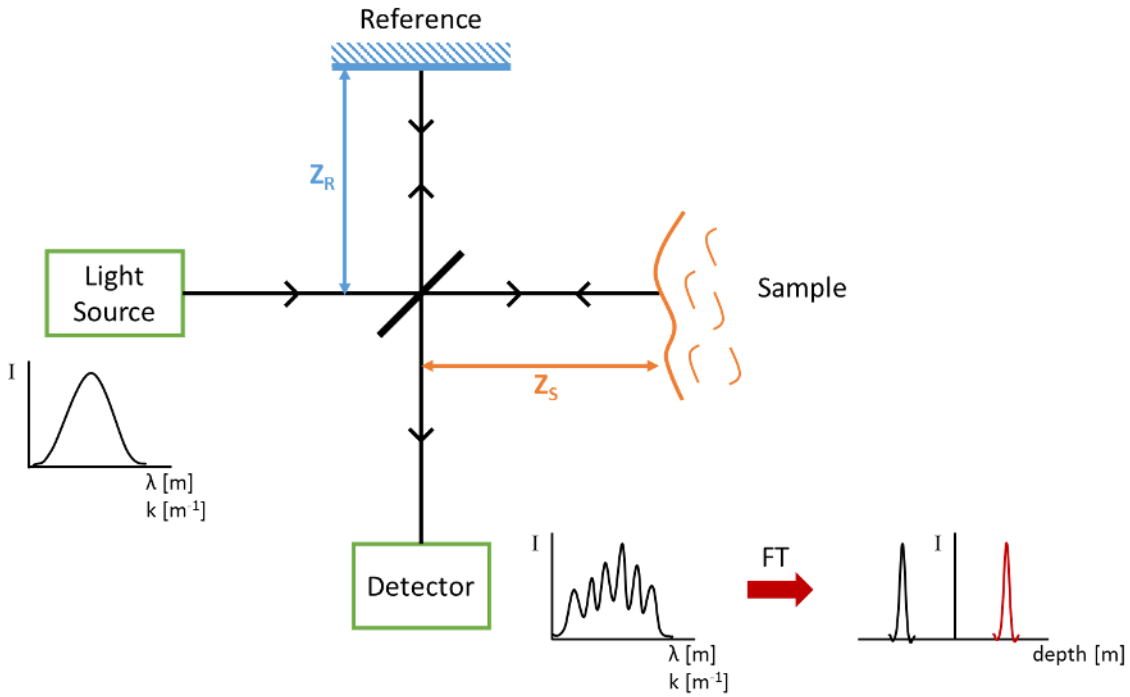

Figure 2 – A schematic detailing the principles of an SD-OCT setup. A broadband spectrum of NIR light is incident onto a beam splitter, which sends one beam up to the reference mirror and the other over to the sample. The light reflected back from both the reference and the sample are collected back at the detector, and this produces Intensity as a function of wavelength/wave number, which can be Fourier transformed into an Intensity versus depth plot.

Since a broadband light source is used with SD-OCT, the backscattered intensity as a function of depth for the entire length of an A-line can be obtained all at once, without needing to scan the reference arm as in time-domain OCT. As mentioned earlier, by transverse scanning of the source beam, many A-lines can be collected and produce a B-scan, or image. OCT can also be used to generate volumetric data by scanning in the third-dimension. Through SD-OCT, the simultaneous acquisition of all the intensities of complete A-line significantly speeds up acquisition time, making this technology more useful for clinical applications. Due to this increase in efficiency compared to time-domain OCT, SD-OCT is more sensitive by several orders of magnitude, permitting greater detection of weak signals and thus generating a more representative image of the tissue[11].

The main benefit of using broadband light source is that the axial resolution Δz of the system can be increased due to the following relationship[7,12,13]: $\Delta z = \frac{2ln2}{\pi}\frac{\lambda_0^2}{\Delta\lambda}$, with λ_0 representing the center wavelength and $\Delta\lambda$ being the full-width half-maximum of the spectrum. Therefore by increasing the spectra bandwidth, a higher axial resolution can be obtained. A drawback of OCT is that the penetration depth of such NIR light is only a few millimeters, and there is significant signal attenuation due to the scattering of light within the tissue. This limits the application of OCT to thin tissues and organ linings, such as the esophagus, colon, cervix, and blood vessels[7].

1.3 Clinical Applications

As mentioned in Section 1.1, OCT has had significant impact in the ophthalmic field, specifically with the imaging of posterior eye segments including the retina, macula, and the optic nerve, allowing for the diagnosis and monitoring of relevant diseases[14].

Recent innovation in spectral-domain OCT has now allowed for the choroid to be visualized and measured, a structure whose changes are implicated in various pathologies[14]. OCT can be used to distinguish between different eye diseases through choroidal thickness measurements; in age-related macular degeneration, the choroid thins significantly compared to healthy eyes whereas in central serous chorioretinopathy, there is a substantial increase in choroid thickness (**Figure 3**)[14]. Monitoring choroidal thickness deviations in addition to various other eye structural properties through OCT has allowed for better understanding and treatment of posterior segment diseases[14].

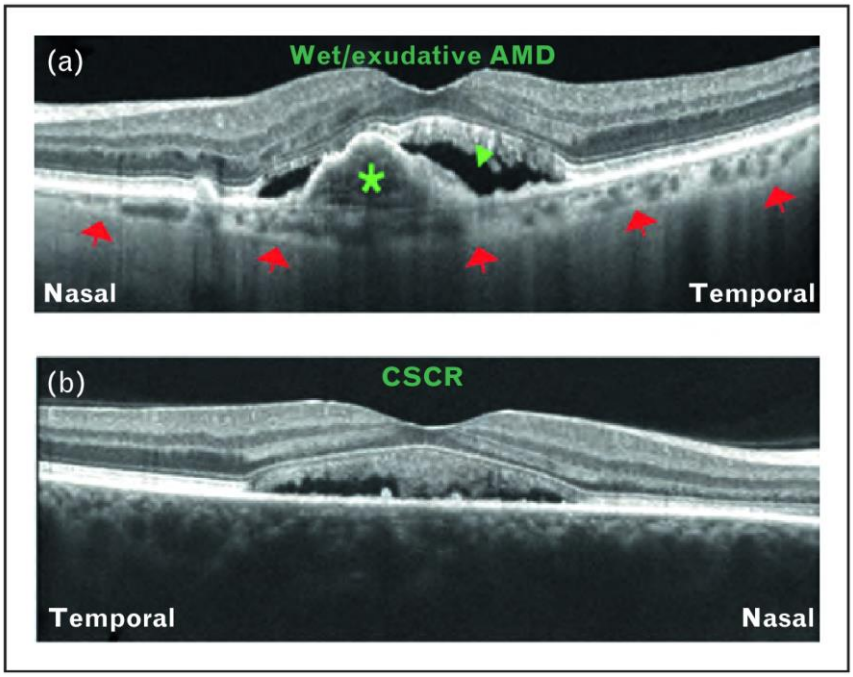

Figure 3 – Using choroidal thickness as a parameter for disease differentiation with OCT. **(a)** OCT image showing wet/exudative age-related macular degeneration (AMD), as indicated by epithelial detachment (green asterisk), collection of subretinal fluid (green arrow), and a thinner choroid observed at the choroid-sclera interface (red arrows). **(b)** OCT image showing a thickened choroid and the loss of visualization of the choroid-sclera interface, indicative of central serous chorioretinopathy (CSCR). These OCT images are approximately 1 mm in depth and 2.5 mm in length. Reproduced with permission from reference [14].

Intravascular OCT (IVOCT) has become an emerging technology in an effort to produce real-time assessment of potentially diseased vasculature. The OCT probe is introduced into the artery via a guidewire, and since blood is impenetrable to NIR light, the field of view must be flushed with a crystalloid/radiocontrast solution in order to produce an image[15]. Due to the high resolution of OCT, these images have some similarities to histological slides and this allows for the cautious use of pathological descriptors when analyzing OCT images[15]. Lesions and various forms of plaque that develop within arteries produce distinct signals through differences in backscattered intensities, allowing IVOCT to distinguish unstable lesions and ruptured plaques[15]. IVOCT can also be used for the assessment of stents by detecting prolapse, thrombus, strut coverage and restenosis (**Figure 4**)[15]. Accurate quantitative measurements of arterial layers, lesion parameters, and stent measurements have been accomplished through IVOCT[15], providing further evidence that OCT has robust potential as a diagnostic tool for cardiovascular applications.

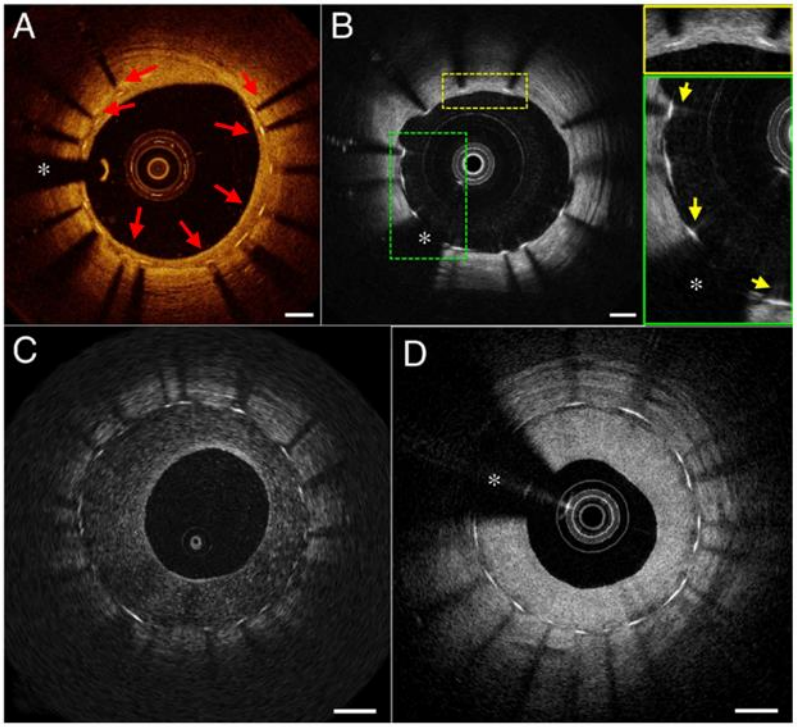

Figure 4 – **(a)** OCT scan of covered stent struts (red arrows). **(b)** OCT scan including both covered (yellow dotted box) and uncovered (green-dotted box) stent struts. Restenosis can present in OCT scans as either a signal-poor **(c)** or signal-rich **(d)** tissue. Reproduced (permission not needed) from reference [15].

Catheter-assisted OCT has also been implemented for esophageal-guided biopsy in the form of volumetric laser endomicroscopy (VLE)[16]. A volume scan is obtained by helically scanning an OCT laser over an extended length of the esophagus; a high-power laser is then used to visibly mark the regions of interest for biopsy[16]. In this study conducted by Suter et al., OCT criteria previously published were used to determine where to mark for biopsy of squamous mucosa, columnar-lined esophageal mucosa, or both, and histology slides of the biopsy confirmed that these criteria and VLE method were sufficient in identifying such regions (**Figure 5**)[16]. Such methods could potentially replace the current gold standard of endoscopy-assisted random biopsy for a more accurate diagnosis of Barrett's esophagus and perhaps carcinoma[16].

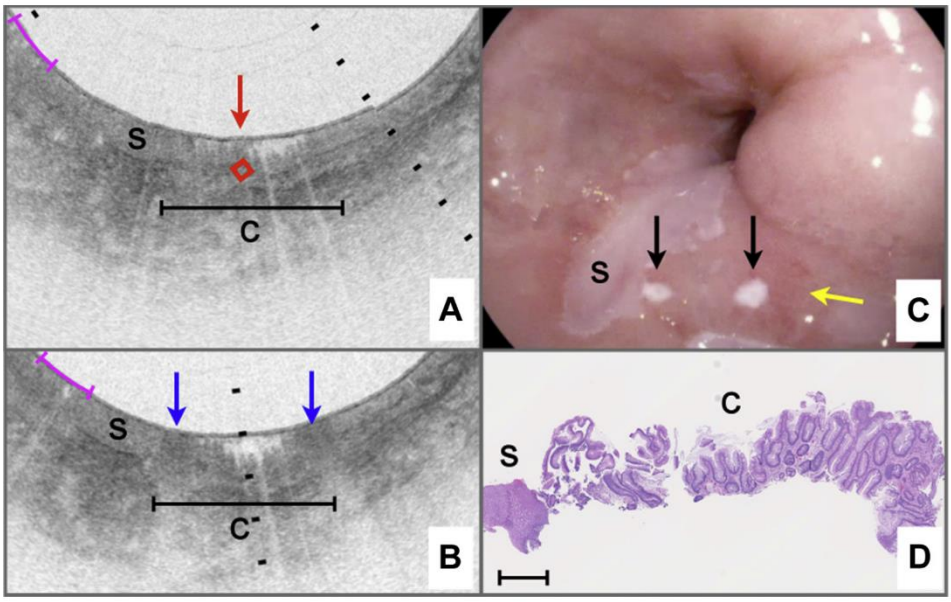

Figure 5 – **(a)** The intent-to-biopsy region containing OCT features of columnar-lined esophagus (indicated by the C, and the center of this region indicated by the red arrow and diamond), bordered with squamous mucosa (S). **(b)** Post-laser marking, the cauterized mucosa appears as darkened areas (blue arrows) in OCT image. **(c)** Videoendoscopy image showing the laser marks (black arrows) within the reddened mucosa (yellow arrow). **(d)** Histology slide of biopsy taken from the marked region, confirming the columnar-lined esophagus with a small section of squamous mucosa. Reproduced with permission from reference [16].

1.4 Dental Applications

In 1998, Colston *et al.* were the first to image dental hard and soft tissue both *in vitro* and *in vivo* using OCT[17]. Since then with the advancement of spectral domain OCT, much research has been done in the dental field, specifically with imaging teeth. *In vitro* work has allowed for the investigation of demineralization of the enamel, providing insight into what causes it, how quickly it can occur, and what features can be detected with OCT. Furthermore, efforts have been made to remineralize the enamel and the success of these developments can be assessed through OCT, permitting product validation. *In vivo* OCT imaging also has great potential for clinical use, allowing for the assessment of tooth

fractures, caries, demineralization, and perhaps even periodontal conditions. This section will explore several of the various research efforts of OCT in dental applications.

Enamel is a typically birefringent tissue, which can be attributed to the hydroxyapatite crystal organization[18,19]. The birefringence of the tissue changes with demineralization and the eventual formation of caries lesions, leading researchers to investigate the use of polarization-sensitive OCT (PS-OCT); this allows for the collection of both refractive index and polarization information, providing a more comprehensive assessment of tooth structure[19,20]. For PS-OCT, rather than generate a backscattered intensity profile as a function of depth, the degree of birefringence as a function of depth is obtained[20,21]. This can be accomplished either by using a pair of detectors to receive the two perpendicular polarization channels, or by using a rotating wave plate and a single detector[18]. Caries increases the backscattering of NIR light and has also been found to depolarize light when the incident light is polarized[22,23]. Research conducted by Fried et al[22] confirmed this relationship. The perpendicular-axis PS-OCT scans show a clear increase in intensity and depth of the lesion with greater contrast than the parallel-axis[23]. This work supports the notion that PS-OCT can help non-invasively detect the formation of these lesions quite early on in the process, allowing for proper diagnosis and quick treatment.

For some applications PS-OCT is not necessary to efficiently observe the more severe dental defects, as demonstrated by a study conducted by Shimada et al. where they compared swept-source OCT scans to conventional X-rays used at the dentist for assessment of tooth health[24]. What was observed through visual examination as a dark spot was imaged using X-ray, and the scan did not indicate the presence of caries; however,

with OCT the DEJ shows high reflectivity in addition to the presence of another highly reflective feature[24]. The results from these studies support the claim that OCT offers higher sensitivity than conventional X-ray and also eliminates the exposure to harmful radiation[24].

In a more recent study by Shimada et al., they further investigated the use of OCT in diagnosing cracks, caries, and restoration defects[5]. The presence and extent of caries can be detected with OCT through increased scattering, and the dentin-enamel junction (DEJ) also becomes highly reflective and distinctive once caries has penetrated this juncture and can help determine the depth of demineralization and the progression of caries into the dentin[5]. Another study by Lenton *et al.* also exhibited the ability of OCT in diagnosing dental issues through the detection of demineralization and caries as areas of high reflectivity, indicating failure of resin composite fillings (**Figure 6**)[25]. These conclusions along with the micron resolution and millimeter imaging depth make OCT a frontrunner technology for the assessment of dental tissue in both research and clinical applications. Compared to other clinical applications, relatively little work has been reported in terms of assessing gingival / periodontal tissue health using OCT.

This thesis work was focused on using OCT for dental and periodontal imaging, specifically for assessing enamel demineralization and gingival inflammation, two early indicators of disease.

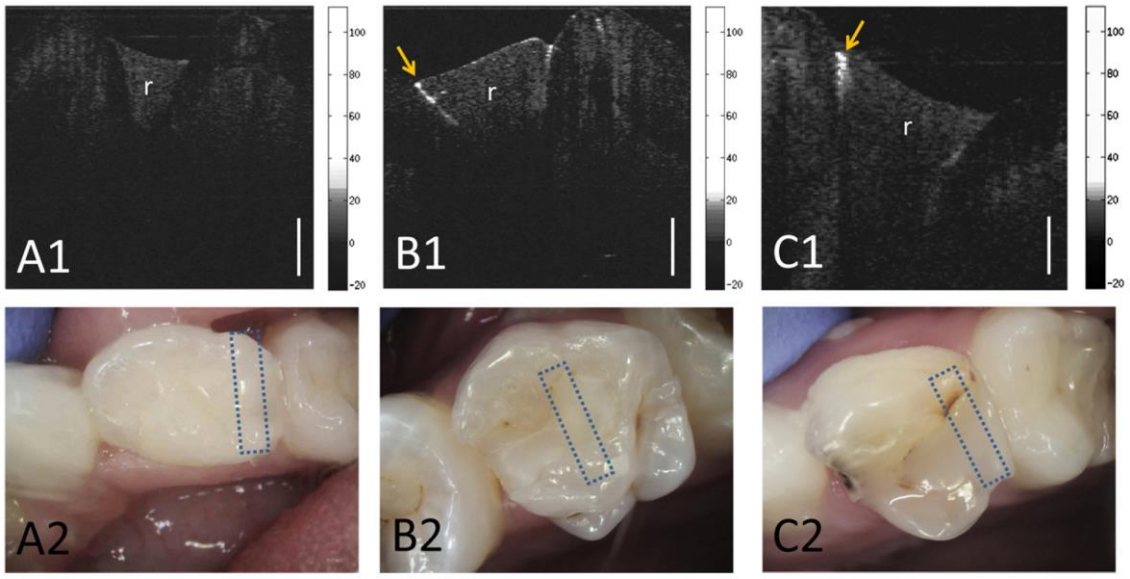

Figure 6 – **(A1)** Cross-Polarization OCT (CP-OCT) image and **(A2)** intraoral photo of a recently completed resin composite filling (**r**). **(B1)** CP-OCT image and **(B2)** intraoral photo of a resin composite restoration that had been placed over 6 months prior. The high scattering (yellow arrow) signifies early failure of the filling as a result of demineralization. **(C1)** CP-OCT image and **(C2)** intraoral photo of a restoration with cavitated secondary caries, also presenting as high reflectivity (yellow arrow). Reproduced with permission from reference [25].

CHAPTER 2: ASSESSMENT OF ENAMEL DEMINERALIZATION USING OCT

2.1 BACKGROUND

2.1.1 PATHOLOGY OF DEMINERALIZATION

Dental caries is a disease caused by normal oral bacteria and presents as a carious lesion that is the ultimate result of demineralization of the enamel, and then dentine, of the tooth[26]. Remineralization of this tissue often follows, but it is when demineralization exceeds the remineralization process that cavitation occurs[26]. Certain factors can make a tooth more susceptible or not to caries formation, with the first being host factors; the enamel contains variations in mineral content, which can make one region more susceptible to demineralization than another[26]. Saliva plays a major role, preventing the dissolution of enamel by removing food debris and loose micro-organisms, neutralizing acids, and providing a source of ions essential for the remineralization process[26]. Fermentable carbohydrates such as sucrose are broken down by oral bacteria into end-products that feed bacteria and contribute to the adhesion and formation of plaque, so diet is another determinant of caries development[26]. Plaque microorganisms such as the *Streptococcus mutans* are some of the most acid producing and tolerant species, and by metabolizing carbohydrates they lower the plaque pH and induce the demineralization process[26].

Hydroxyapatite crystals are the major component of enamel, and they are arranged into what is referred to as *enamel prisms* which contain about 1000 crystals each[27]. The interface between prisms often provides greater intercrystalline space and is consequently more susceptible to diffusion of demineralization-causing solutions[27]. Additionally, the distribution and arrangement of the crystals and prisms is not uniform across the tooth surface, making certain areas more susceptible to disease[27]. Enamel demineralization is

the result of dissolution of these hydroxyapatite crystals, and can happen either from the center of the crystal structure or from the periphery[27,28]. This dissolution results in a roughening of the crystal structure and the formation of pores which can eventually lead to the development of carious lesions[27,28].

2.1.2 DETECTION OF DEMINERALIZATION USING OCT

The roughened tooth surface created by crystal dissolution has an effect on the reflectivity of the enamel, which allows for demineralization to be detected through OCT. This imaging modality has been used to assess demineralization quite extensively *in vitro*[29-39]. Early demineralization has been studied either on extracted teeth with visible carious lesions or white spots[30,32,38] or by simulating demineralization of bovine or human tooth samples through the use of a demineralizing solution, with the most common ones being (1) a calcium-phosphate-acetate solution[29,31,33,34,39], (2) a methylcellulose gel with lactate buffer[35,36], and (3) orange juice[33,37]. The duration of demineralization also varies across studies, ranging from hours[34,37] to a few days[31,33,39] to about two weeks[29,33,35,36,39]. All of these studies investigate the ability of OCT in detecting demineralization, and some have compared their results to other technologies, including polarized light microscopy[29,34,39], confocal laser scanning microscopy[32,38], nanohardness[35] and microhardness[37]. Such comparisons have allowed for firm conclusions that OCT can dependably distinguish enamel demineralization. The work conducted by Chew *et al.* was of particular interest for this thesis, as these researchers were focused on investigating early enamel erosion and specifically the dose-dependent demineralization response with OCT[37]. Their results

suggest that this modality could be utilized as an *in vitro* method of monitoring progression of the early demineralization process[37].

In vivo evaluation of demineralization has been less extensively investigated[25,36,38,40-42]. Shimada *et al.* recently reviewed the various applications of OCT in dentistry, including the detection of demineralization as well as the diagnoses of cracks, caries, and restoration defects[5]. Several studies have focused on imaging caries *in vivo* as an alternative means of diagnosis, identifying these lesions as brighter enamel regions in the OCT images[5,24,25,38,42]. Other researchers have investigated how OCT can be used to assess how certain products affect enamel erosion, whether it be orthodontic brackets contributing to demineralization[41] or treatments, such as fluoride, to prevent or reverse demineralization damage[36,40].

The long-term goal of my lab's research is to be able to translate this technology to the clinical setting where both early demineralization and remineralization can be evaluated *in vivo*. In order to reach this objective, the ability of the current OCT setup in detecting enamel demineralization must be tested and established *in vitro* prior to performing *in vivo* measurements. The aim of this chapter is to determine if a time-dependent demineralization response of bovine enamel can be induced and detected with OCT using 30% H_3PO_4 (phosphoric acid) as the demineralizing solution. Phosphoric acid is commonly used for etching the enamel prior to the application of bonding resins[43], and is also an additive to soft drinks for both taste and preservation purposes[44]. As a result, this acid was the demineralization solution chosen for the following experiments. In addition to OCT, microhardness will be used to confirm or deny a time-dependent relationship as well as establish any correlation between the two technologies[35,37].

2.2 HYPOTHESIS

OCT can measure the intensity of backscattered light arising from micro-scale refractive index mismatches in surface and sub-surface layers in biological tissues. Demineralization is known to alter the structure of dental enamel, creating a microscopically roughened surface which exhibits qualitatively different scattering at the macroscopic (visual) scale. I hypothesize that OCT can quantify demineralization of tooth samples *in vitro* by measuring the intensity of backscattered light from the enamel surface. If successful, this technique could potentially be translated to *in vivo* assessment of enamel demineralization and remineralization.

2.3 METHODS

To determine the ability of OCT to detect enamel demineralization, dilute phosphoric acid was used to induce demineralization in bovine tooth samples. Each sample was submerged in the acid solution to achieve 3 levels of exposure: 0 sec, 2 sec, and 5 sec. Following acid exposure, OCT images were acquired, and backscattered light intensity as a function of depth was analyzed for each time exposure. As a gold standard test for demineralization, microhardness indentation was performed on the samples. To test the above hypothesis, quantitative OCT intensity values were compared to microhardness values for each sample and statistical analysis performed (detailed below).

2.3.1 DEMINERALIZATION PROCESS

In order to induce demineralization *ex vivo*, 30% H_3PO_4 (diluted from 85% stock, Sigma Aldrich) and 6 bovine tooth samples (approximately 5mm x 5mm x 2 mm) were used. For demineralization, 8 ml of 30% H_3PO_4 was transferred to a single well of a 6-well plate. The sample was divided into three sections depending on exposure time in the acid (**Figure 7**). In order to separate the sample into these sections, yellow electrical tape (3M) was used as a protectant in order to provide 3 sections of exposure to acid: 0 sec, 2 sec and 5 sec.

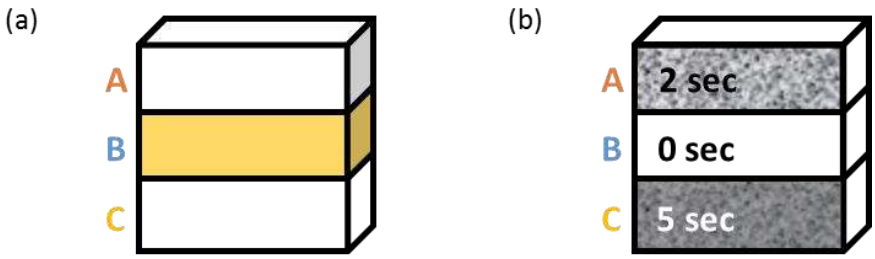

Figure 7 – **(a)** Schematic of how the sample was prepared prior to acid exposure. The middle third of the tooth was protected with yellow tape. **(b)** After demineralization and tape removal, the tooth will have these three sections, labeled A (2 sec), B (0 sec), and C (5 sec).

An alligator clip was used to securely hold the sample and dip it into the diluted phosphoric acid solution, making sure to submerge only the exposed region of the tooth to help minimize acid seeping underneath the tape. A schematic depicting the demineralization process is provided in **Figure 8**. After the desired exposure time, the sample was removed from the demineralization solution and immediately rinsed under a running reservoir of ddH_20 for 1 minute, dabbed dry with a Kimwipe and then dried with forced air for 20 seconds. The protective tape was removed from the 0 sec exposure region and the sample was ready for OCT imaging with a gradient of exposure to phosphoric acid.

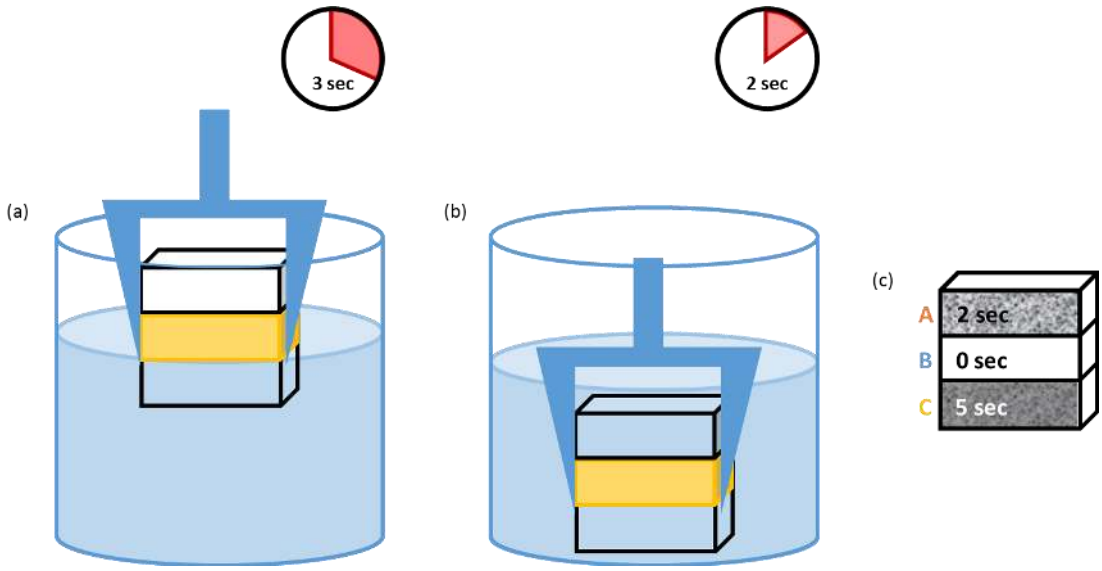

Figure 8 – Schematic of demineralization process. **(a)** The bottommost third of the sample is dipped into the 30% H_3PO_4 for 3 seconds. **(b)** Immediately after the 3 seconds, the whole tooth sample is submerged in acid for 2 more seconds. After rinsing and drying, tape is removed from the control region and the tooth has exposure regions of 2 sec, 0 sec, and 5 sec **(c)**.

2.3.2 BENCHTOP OCT HARDWARE

The SD-OCT system uses a fiber-coupled superluminescent diode light source (Thorlabs) with 1325 nm center wavelength and 100 nm bandwidth (full-width at half maximum). The source is connected to a fiber-optic circulator which directs light to a fiber-optic splitter, sending 90% of source light to the sample and 10% to the reference arm. The sample arm contains a 2-axis galvanometer scanner (Thorlabs) and a 60 mm focal length lens to focus light into the sample. The reference arm contains a variable neutral density filter to adjust the reference light intensity, and a stationary mirror. Light returning from the sample and reference arms is recombined at the splitter and directed to a spectrometer for detection. The spectrometer comprises a 50 mm collimating lens, a 1145 lines / mm diffraction grating (Wasatch Photonics), and a 100 mm focal length lens

to focus the spectrally dispersed light onto a 1024 pixel InGaAs line-scan camera (UTC Aerospace Systems, Princeton NJ). Using the spectrometer's previously established pixel-to-wavelength calibration, we obtain measurements of signal intensity as a function of optical wavelength (I(λ)). Data was transferred to PC via a CameraLink frame grabber board (National Instruments), with all data acquisition and storage controlled by LabVIEW software developed in-house. This setup is depicted both schematically (**Figure 9a**) and physically (**Figure 9b**) below.

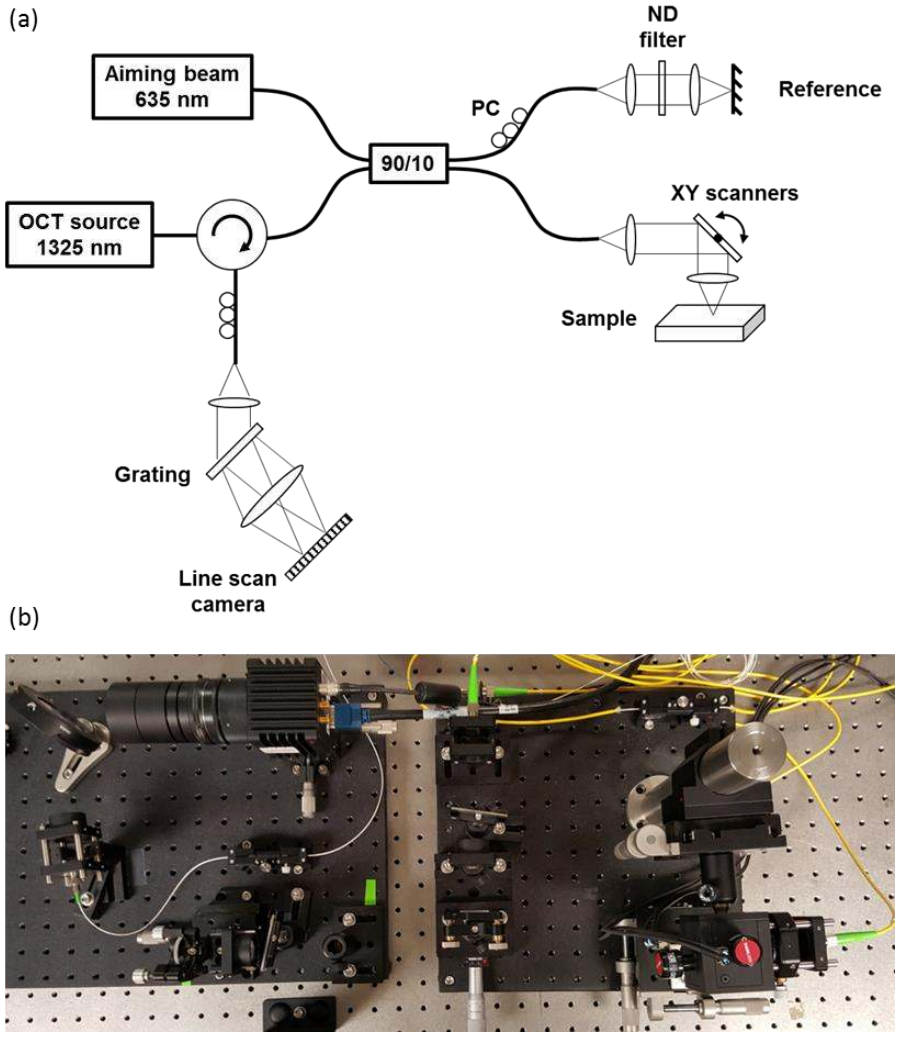

Figure 9 – Schematic **(a)** and picture **(b)** of the benchtop OCT setup.

2.3.3 OCT DATA ACQUISITION

Prior to demineralization, the surface of these bovine samples is highly reflective and can produce large artifacts appearing as "echoes" in the OCT B-scans due to specular reflection if the sample is imaged with the beam directly perpendicular to the surface (**Figure 10a**). However, by slightly tilting the sample, this artifact can be eliminated and a clean image of the surface and underlying structure is obtained (**Figure 10b**). To apply this tilt easily and consistently between samples, a sample holder was designed and 3D printed (**Figure 10c**). The tooth is placed so that the top-right portion of the sample fits into the corner of the holder and is flush against the sides, and the sample is tilted down into the holder. This tilt successfully eliminates specular reflection artifact, and the holder helps keep the sample steady and in the same position for each measurement. For OCT image acquisition, the scanning beam acquired 500 A-lines per 7-mm wide B-scan, and 500 B-scans were taken over 7 mm in the transverse direction.

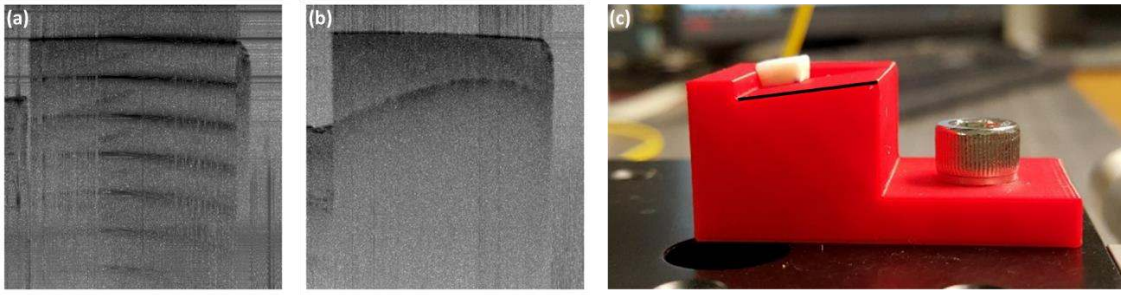

Figure 10 – **(a)** OCT image of a flat bovine sample with no tilt. **(b)** OCT scan of the tilted bovine sample. The 3D printed tooth holder **(c)** was used to provide a consistent tilt to all imaged samples.

2.3.4 OCT DATA ANALYSIS

Although the bovine samples were polished flat, they still have surface variations across the sample as demonstrated in the previous section. To compensate for this, the enamel surface was detected using the MATLAB Canny edge detection function (**Figure 11a**). Canny edge detection first eliminates noise by smoothing the image through Gaussian convolution. Then hysteresis thresholding is implemented with upper and lower thresholds. A pixel is accepted as an edge if its gradient is greater the upper threshold and it is rejected if it is below the lower threshold. When the gradient falls between the two values, the pixel will be accepted if it is connected to a pixel above the upper threshold, otherwise it will be excluded. The detected surface was then realigned to the top of the image, providing an even surface from which the intensity versus depth profile of the tissue can be analyzed, independent of lateral location (**Figure 11b**).

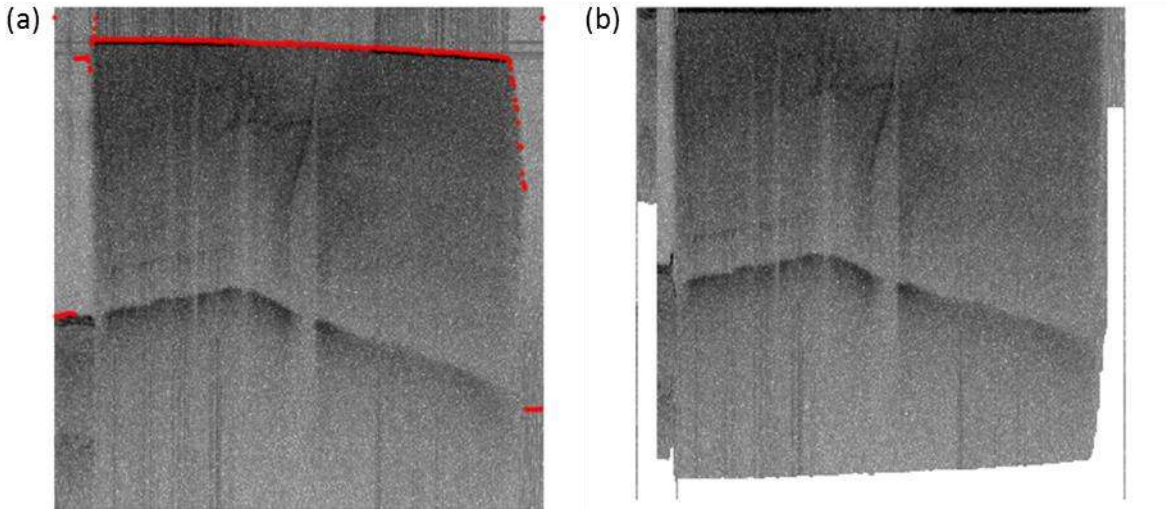

Figure 11 –OCT image of a bovine tooth sample. **(a)** Enamel surface detected with MATLAB's Canny edge detection algorithm (red line). **(b)** Realignment of detected surface to the top of the image, generating an even surface to perform Intensity vs. depth analysis.

The region of interest for analysis was next selected from one of the B-scans by the user by means of the MATLAB function *ginput*, and an intensity versus depth profile was generated from the average of these selected A-lines (**Figure 12**). Note that for all OCT images presented in this chapter, a strong backscatter signal is mapped to black, and weak backscatter to white, in a continuous grayscale colormap.

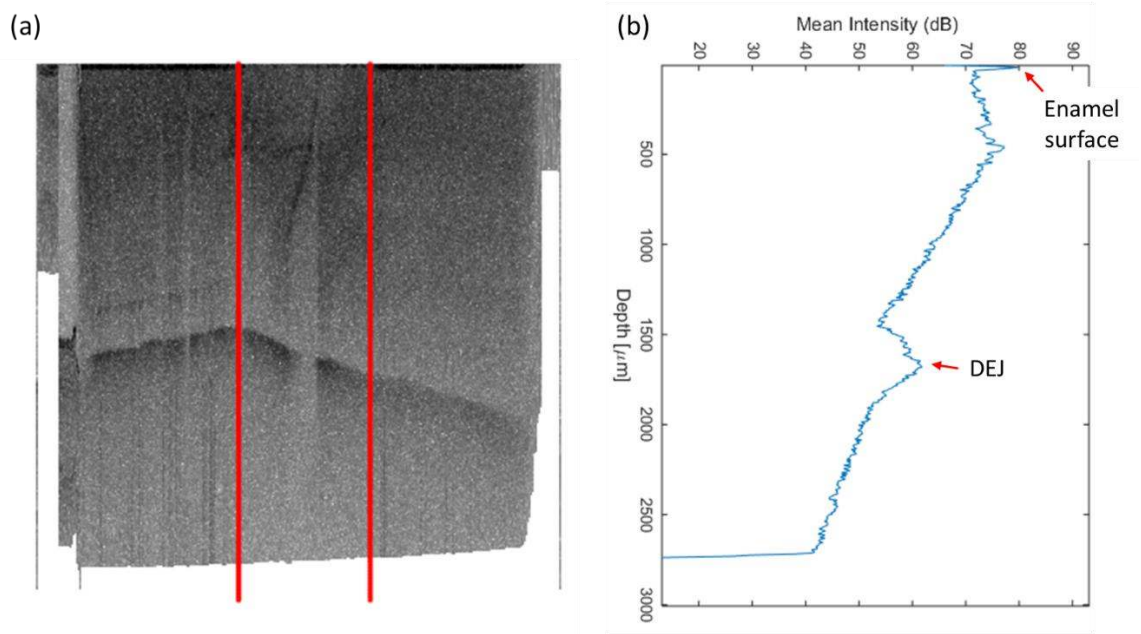

Figure 12 – **(a)** OCT image of a bovine tooth sample realigned to the enamel surface. The region of interest is between the two red lines. The backscattered intensity is averaged over the number of A-lines between the red lines in **(a)** and this mean intensity is plotted as a function of depth **(b)**.

Due to natural variations in tissue composition, the backscattered intensity can vary depending on the OCT scan location. This was demonstrated by comparing intensity profiles from six separate B-scans, spaced 25 scans (~0.36 mm) apart (**Figure 13a**). As can be seen, there is significant peak/surface variation across the sample, with a 5.75 dB difference over approximately 2 mm. Since these peak values are of significance in this

study, 6 B-scans spaced 15 B-scans apart, covering approximately 1.3 mm, were used (**Figure 13b**) and the intensity vs. plots were averaged together to accommodate for these disparities.

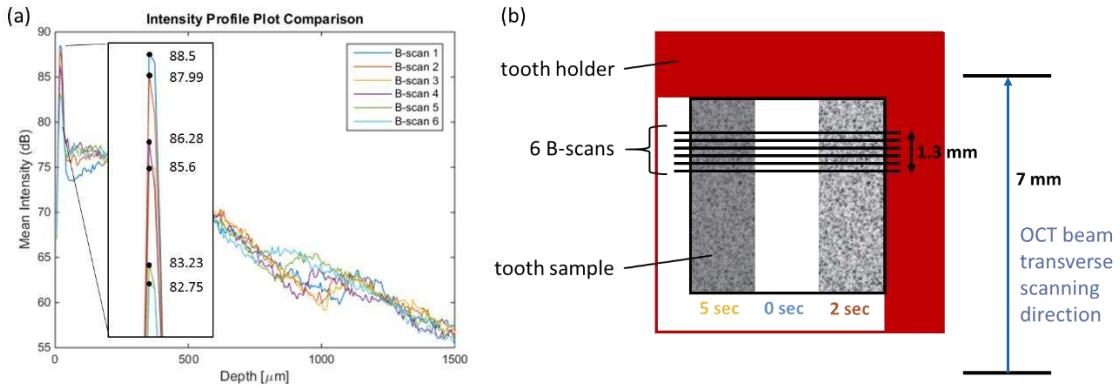

Figure 13 – **(a)** Mean backscattered intensity profiles for 6 B-scans, spaced 25 B-scans apart, from an untreated bovine sample. **(b)** Schematic of how the treated tooth is placed into the tilted tooth holder. The OCT transverse scanning is indicated in this schematic, and the 6 B-scan selections are identified.

The region of interest was manually selected for all exposure sections of the sample, which in **Figure 14a** was 2 sec, 0 sec, and 5 sec going from left to right. The written MATLAB script then went through the 6 selected B-scans and analyzed these regions by producing mean intensity profiles as a function of depth for each exposure section. The 6 profiles were then averaged together to minimize variations due to location for each time point, and these 3 final profiles (0 sec, 2 sec, and 5 sec) were plotted together for comparison (**Figure 14b**). The intensity values for these plots were automatically written to an Excel sheet, and two values were extracted for further analysis: ***peak intensity value*** and the ***percent difference in the decay of backscattered intensity*** (ΔD).

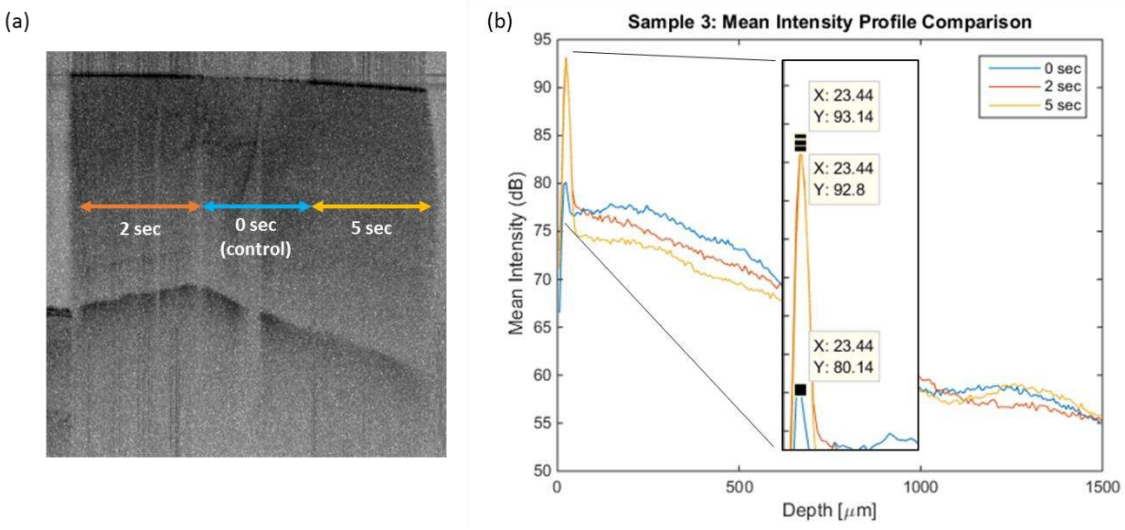

Figure 14 – **(a)** OCT image of treated bovine sample 3, with the 2 sec, 0 sec, and 5 sec exposure regions indicated with color-coded arrows. **(b)** Mean backscattered intensity profiles, averaged over 6 B-scans, for each exposure time as a function of depth. A zoom in on the peak intensity values is provided in the pop-out box.

Acidic solutions demineralize enamel through the dissolution of hydroxyapatite crystals, and this process roughens the tooth surface. This phenomenon should result in an increase in surface backscattering and a reduction in OCT signal below the surface. Therefore, the OCT intensity vs depth profiles were investigated to determine if the increasing acid exposure times resulted in these expected changes in backscattered intensity. First, OCT peak values were compared between 0 sec, 2 sec, and 5 sec of exposure. Since there are compositional variations within and across samples, ratios of peak ($I_{superficial}$) to plateau ($I_{plateau}$) intensity values (**Figure 15**) were compared to perform an assessment of demineralization that is independent of the sample's native properties.

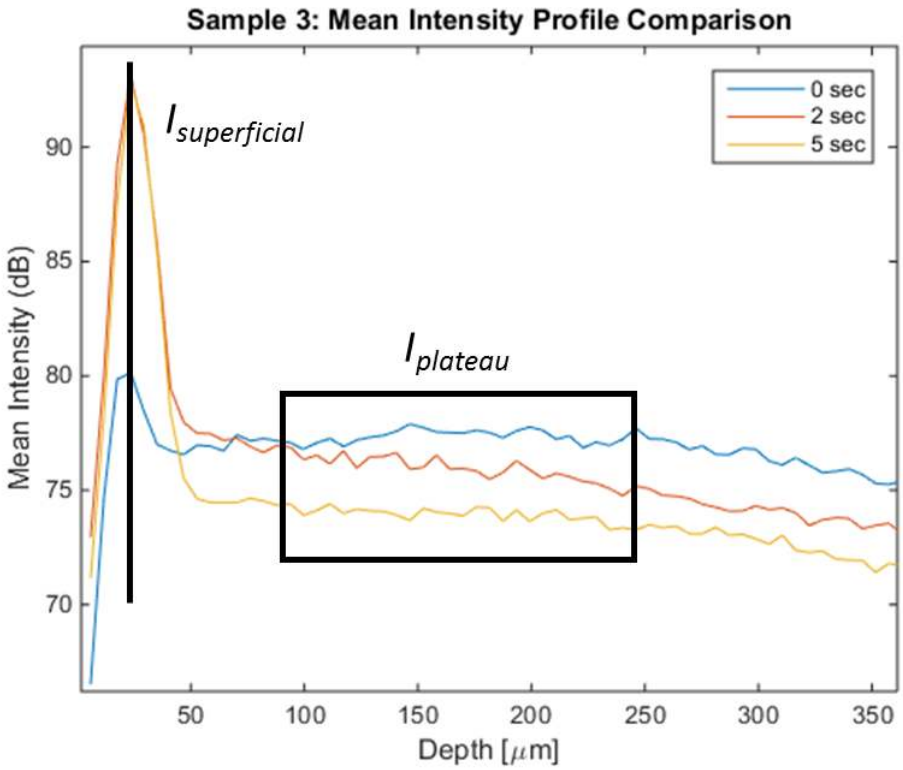

Figure 15 – Mean backscattered intensity profile as a function of depth for bovine sample 3, with the regions used for calculations further calculations indicated, including $I_{superficial}$ and $I_{plateau}$. For $I_{plateau}$, the values within the box were averaged to provide a single intensity value.

The decay of backscattered intensity (D) is equal to the intensity of the plateau, or unaffected region of tooth ($I_{plateau}$), divided by the intensity of the peak, or demineralized enamel surface ($I_{superficial}$). This is calculated for both the non-exposed, or 0 sec, region (D_{NE}) and the exposed regions (D_E). The percent difference of decay of backscattered intensity between the exposed and non-exposed regions (ΔD) is then calculated as[37]:

$$\Delta D(t) = 100\left[\frac{D_E(t)}{D_E(t_0)} - \frac{D_{NE}(t)}{D_{NE}(t_0)}\right].$$

This value should provide a value that corrects for any compositional variations and therefore produce comparable results.

2.3.5 MICROHARDNESS TESTING

As a gold-standard test for enamel demineralization to compare against OCT data, microhardness testing was performed on all samples post-demineralization. A Knoop micro-indenter (Buehler Micromet 6020) (**Figure 16**) was used to incident a 50 g load on the sample surface for 15 seconds, and the subsequent microindentation was measured to produce a Knoop hardness number (*KHN*). Three independent measurements were made per exposure section and these values were averaged together. To ensure that proper readings were taken, the tooth surface was placed orthogonal to the micro-indenter. The ***relative surface microhardness change*** (ΔSMC) (%) was determined from the following equation[37]:

$$\Delta SMC(t) = 100\left[\frac{KHN(t) - KHN(t_0)}{KHN(t_0)}\right]$$

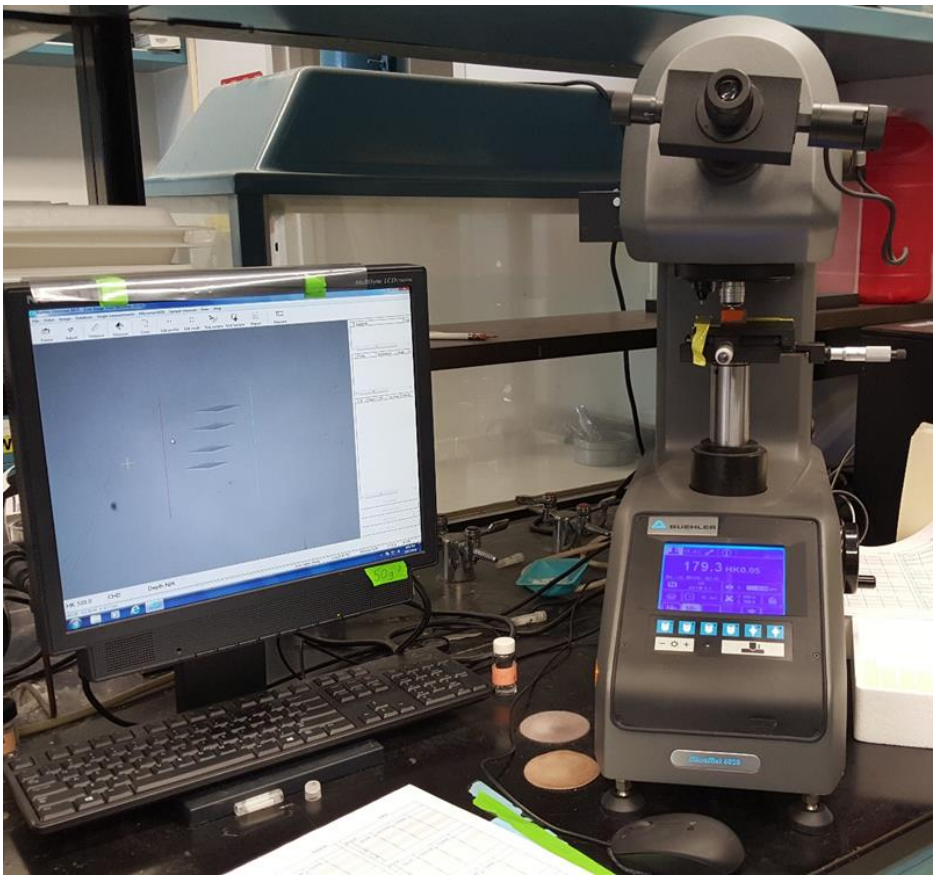

Figure 16 – Knoop micro-indenter setup (Buehler MicroMet 6020), with an example of micro-indentation results on the monitor to the left.

2.4 RESULTS

In order to accommodate for compositional variations within the tooth as well as instrumentation discrepancies, results were expressed as percentage differences relative to the non-exposed regions (ΔD for OCT results, and ΔSMC for the microhardness assay). **Figure 17a** shows the OCT peak backscattered intensity plotted with respect to the duration of acid exposure (0 sec, 2 sec, and 5 sec) for each sample. **Figure 17b** shows the percent difference of backscattered intensity (ΔD) plotted versus exposure time.

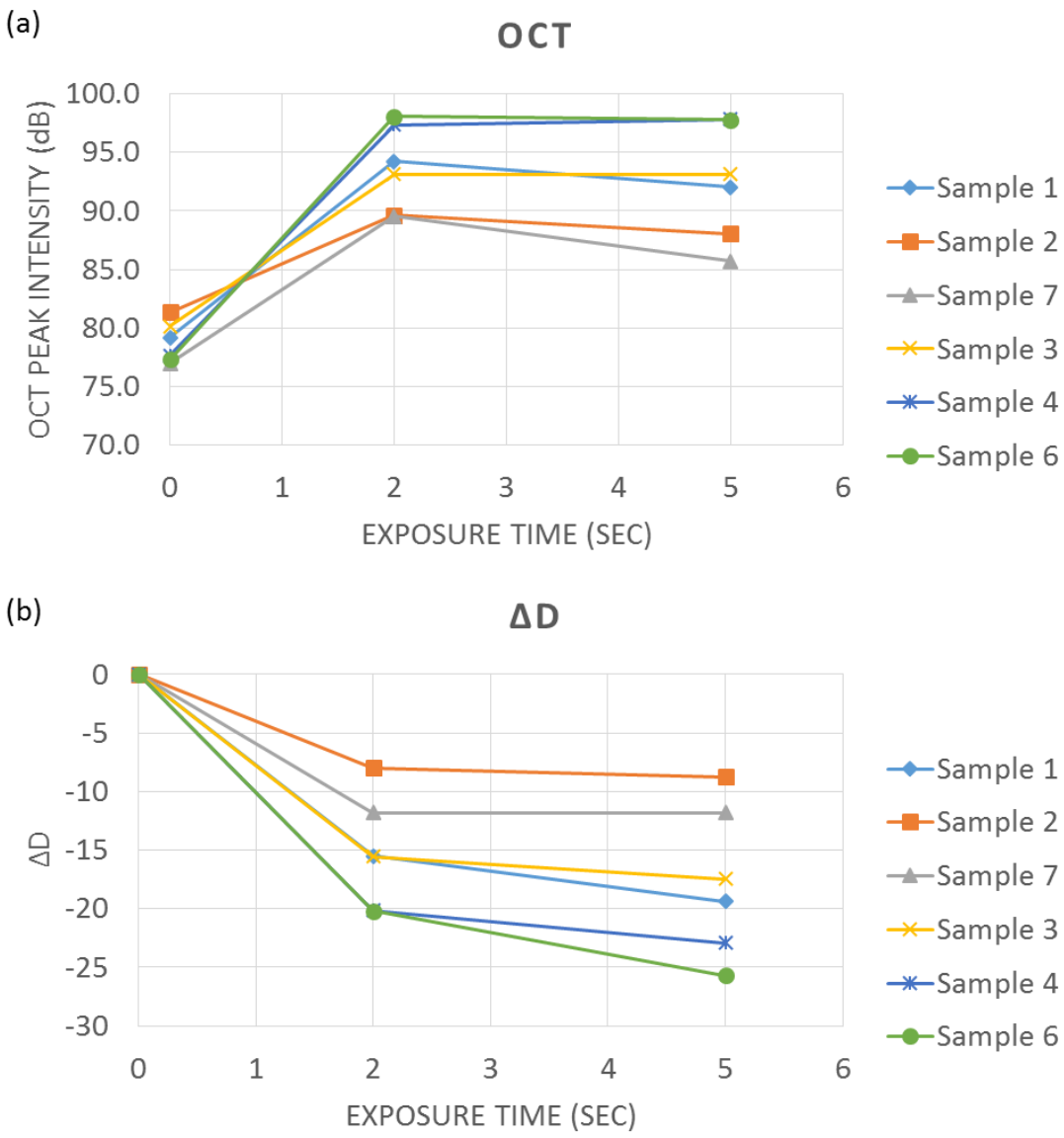

Figure 17 – **(a)** OCT peak backscattered intensity (dB) plotted vs. exposure time (sec) for all 6 samples. **(b)** ΔD plotted vs. exposure time for all 6 samples.

Both of these figures show a significant change between the 0 and 2 second exposure, and a plateau effect between the 2 and 5 second exposures. There is an average reduction in OCT intensity of 15% between 0 and 2 seconds, and 3% between 2 and 5 seconds.

Figure 18a shows Knoop hardness plotted with respect to the duration of acid exposure (0 sec, 2 sec, and 5 sec). **Figure 18b** provides the decrease in percentage change of microhardness (ΔSMC) plotted versus exposure time.

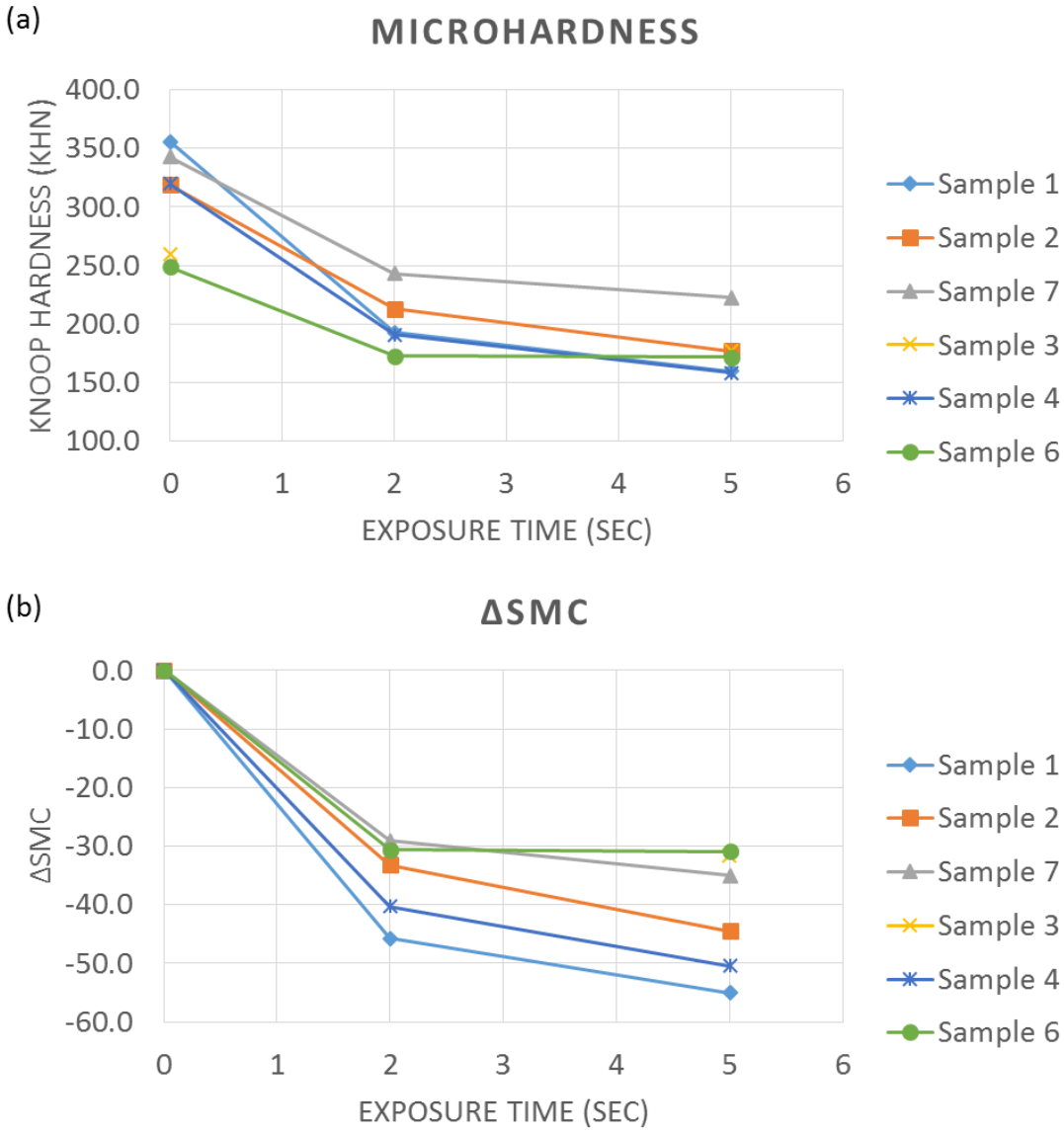

Figure 18 – **(a)** Knoop hardness number (KHN) plotted vs. exposure time (sec) for all 6 samples. **(b)** ΔSMC plotted vs. exposure time for all 6 samples.

Both of these figures also show a significant difference between the 0 and 2 second exposure, and a plateau effect between the 2 and 5 second exposures. There is an average reduction in microhardness of 36% between 0 and 2 seconds, and 5% between 2 and 5 seconds.

To determine the relationship between OCT and microhardness responses to acid exposure, the two were plotted against each other both with raw values (**Figure 19**), and with the corrected percentage differences (**Figure 20**).

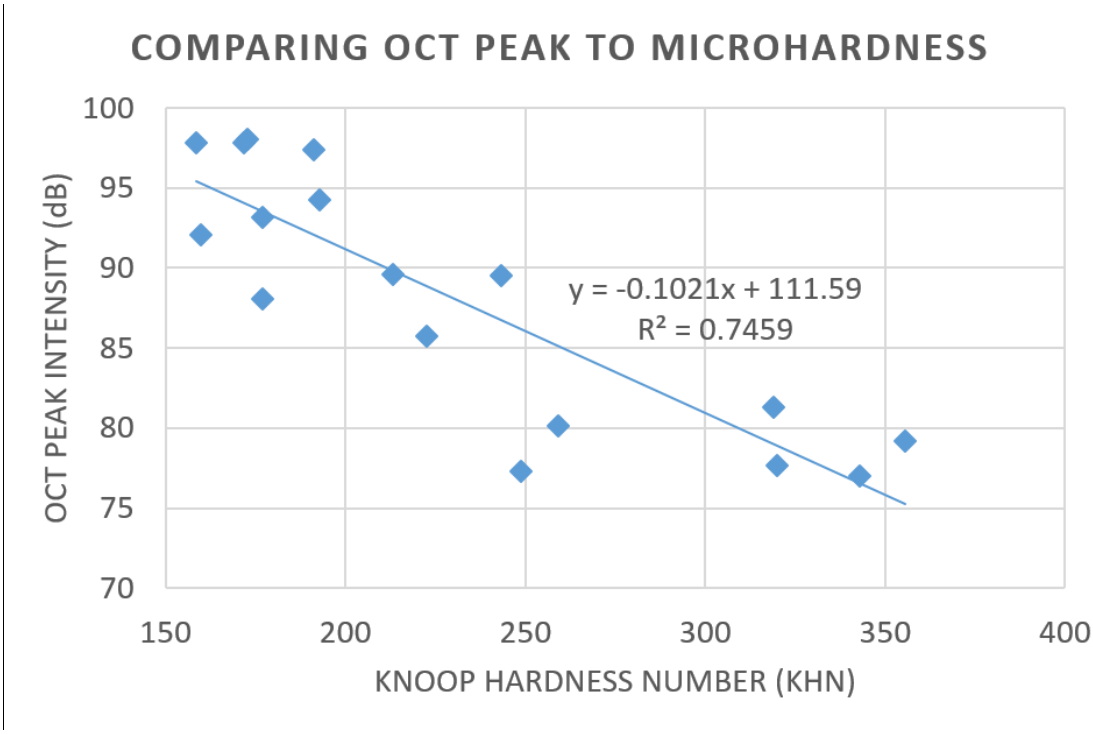

Figure 19 – OCT peak intensity (dB) plotted versus Knoop hardness number (KHN) with a linear trendline plotted to this data.

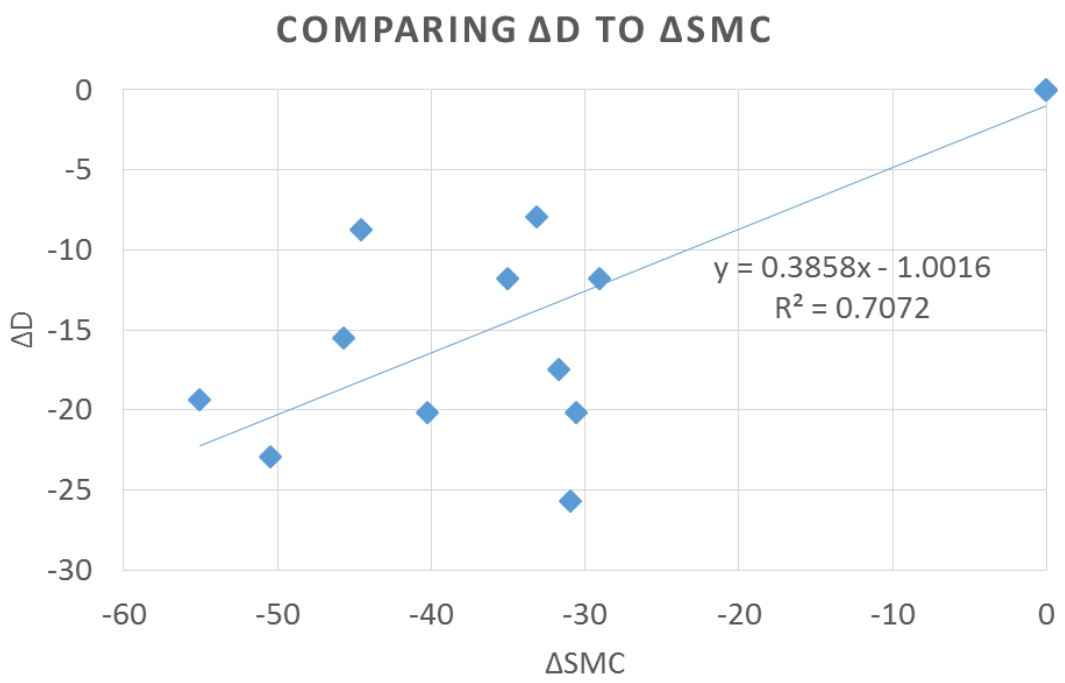

Figure 20 – Δ*D* plotted versus Δ*SMC* with a linear trendline plotted to this data.

To assess whether the data indicated a correlation between microhardness values and OCT values, I started with the null hypothesis (H_0) that *the microhardness and OCT results are independent* (correlation, $\rho = 0$). A linear trendline was fit to the experimental data sample, and the correlation coefficient (r) was obtained. To determine whether H_0 can be rejected, Student's t-test was applied to calculate the probability of obtaining this data sample from a population with a correlation of zero. From these calculations, a statistically significant negative correlation was found between Knoop hardness number and OCT peak intensity ($p < 0.05$), while a statistically significant positive correlation was found between Δ*D* and Δ*SMC* ($p < 0.05$).

2.5 DISCUSSION & CONCLUSIONS

Since the dependence between microhardness and OCT signal is not known, a linear fit was made to the data comparing the two parameters. It is possible that this may not be the best fit, but it was the first choice for these experiments to determine if there is a relationship between the two measurements. Due to the statistically significant correlation calculations, the null hypothesis can be rejected, and I can confirm that changes in OCT signal are correlated with microhardness changes. The data suggest that a substantial change in microhardness could provide a wide range of outcomes on OCT, signifying that while these parameters may be correlated, the strength of this correlation is not strong. This sheds some light on the sensitivity to changes in demineralization which OCT might be able to detect; while micro-indentation testing may be more sensitive to detecting changes in hardness due to demineralization, OCT may not be capable of detecting this change until after a significant reduction in microhardness.

The results of this study also provide two additional conclusions: (1) the diluted phosphoric acid solution effectively induced demineralization, and (2) OCT can successfully detect this demineralization, as confirmed with microhardness testing. This correlation and the understanding of how the OCT setup identifies demineralization allows for confident progression of experimentation into *in vivo* studies.

The aim of this chapter was to determine if there was a time-dependent demineralization response with the use of 30% H_3PO_4. While such a relationship was established, the process was quite swift and aggressive, providing a significant etch in just 5 seconds. To ensure that this dose-response is maintained *in vivo*, further dilution of the

acid must be accomplished to provide a less severe etch over a longer exposure time. This will allow for a more practical window of time to perform OCT imaging clinically.

In this chapter, a coarse volume analysis was implemented by averaging the intensity profiles of 6 B-scans, spaced 15 B-scans apart. Further valuable information may be obtained through a dense volume analysis of all 500 B-scans. Through volume reconstruction of these cross-sectional (XZ) scans using 3D Slicer (NIH), an image of the top surface (XY plane) can be generated through OCT (**Figure 21**).

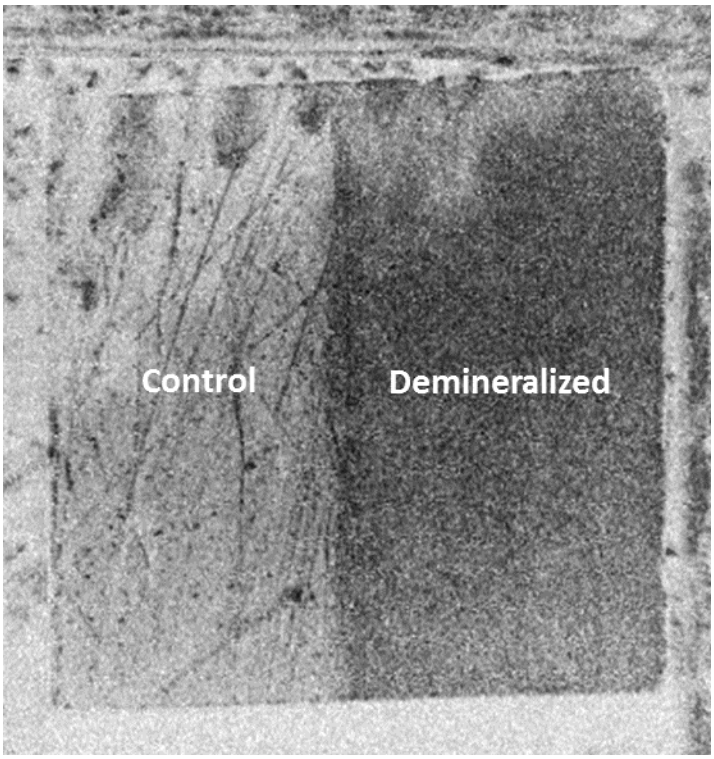

Figure 21 – Reconstruction of 500 cross-sectional (XZ) scans (B-scans) showing an image of the top surface (XY plane) of the entire bovine sample through OCT. This allows for visualization of the control (left) and demineralized (right) enamel surface, as well as visualization of variability and scratches. The tissue sample (5 mm x 5 mm) is positioned in the corner of the sample holder, as shown in Fig. 10c.

Half of this sample was demineralized, while the other half remained protected from the solution, and these two areas can be clearly distinguished in the reconstructed volume. Such a reconstruction provides a visualization of the regional variability of the sample and can be used to make appropriate B-scan selections for the subsequent coarse volume analysis.

For these experiments in which the samples have flat surfaces, they can be tilted to remove the strong surface reflection. Natural tooth surfaces on the other hand have unique curvature and this simple correction cannot be implemented when using a handheld probe *in vivo*. Cross-polarization can be applied instead, as has been done in previous studies[39,45]. For my current setup, the NIR output beam and reflected signal both travel through the same fiber, so in order to achieve cross-polarization a polarizer and wave plate configured at 45° were added to the OCT lens (**Figure 22**).

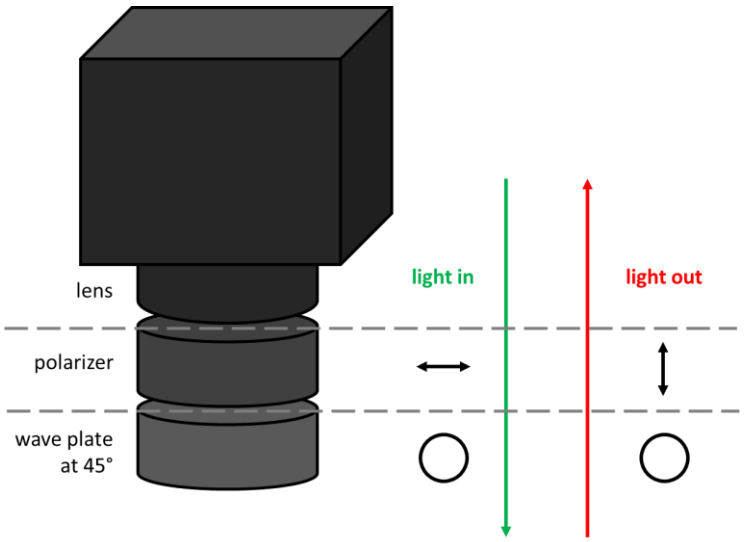

Figure 22 – Schematic of cross-polarization implementation. The polarizer introduces a linear polarization state to the incoming light, and the wave plate turns this into a circular polarization state. The light reflected back from the sample will also be of circular polarization, and when this light comes back through the polarizer, it will be of the opposite polarization of the incident light.

The light is initially in an unknown polarization state, so a polarizer is added to introduce a pure linear polarization state. After this beam passes through the wave plate, it acquires circular polarization and the light that is reflected from the sample is also of a circular polarization state. When it passes back through the polarizer, its state will orthogonal to the incident light. In a regular setup, light reflected off the surface is the same polarization as the incident light; with the cross-polarization modification, the surface reflection will be blocked by the polarizer, as confirmed on human tooth samples (**Figure 23**).

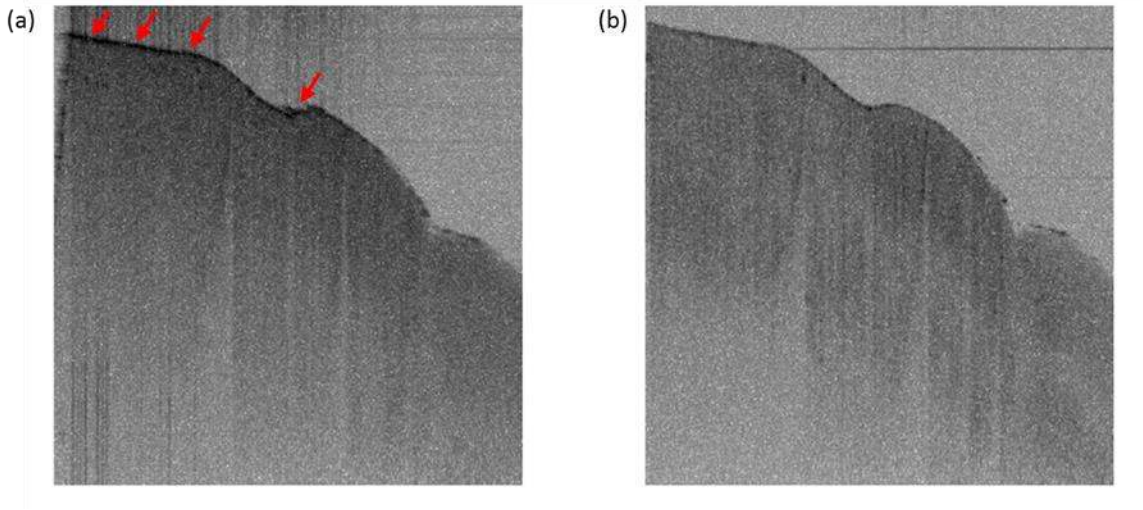

Figure 23 – **(a)** OCT image of a human tooth, with significant amounts of specular reflection (red arrows). **(b)** OCT image with cross-polarization, showing reduced specular reflection.

The high surface reflection, which could be mistaken for demineralization, is eliminated with cross-polarization. Therefore, cross-polarization may be beneficial for future work and for translation into *in vivo* studies.

CHAPTER 3: ASSESSMENT OF GINGIVAL TISSUE WITH OCT

3.1 BACKGROUND

3.1.1 GINGIVAL INFLAMMATION AND DISEASE PROGRESSION

Conditions that affect the supporting structures of the teeth are referred to as periodontal disease, which can be divided into two general categories: gingivitis and periodontitis[26]. The accumulation of plaque microflora near the gingival margin leads to a breach in the host defense followed by gingival inflammation, or gingivitis; if untreated, this can progress to periodontitis with periodontal inflammation and the detachment of the gums from the tooth[26]. These diseases are assessed clinically depending on the disease progression rate and the distribution of lesions as well as on patient age and any comorbidities[26].

The gingival crevicular fluid (GCF) is one of the most significant factors in the response to plaque formation[26]. The accumulation of plaque leads to an inflammatory response and a subsequent increase in GCF, which contains specific and non-specific immune factors[26]. Polymorphonuclear leukocyte (PMNL) numbers, which are minimal in healthy gingiva, surge as they migrate from venules and into the gingival sulcus where they will begin to phagocytose the present bacteria[26]. The antibodies contained within the GCF also indicates the involvement of T-cells and B-cells in this process[26]. While these inflammatory responses are in effort to protect the host from this detrimental bacteria accumulation, the processes also have damaging effects to the tissue and can actually lead to disease progression[26].

Chronic marginal gingivitis is characterized by redness and edema of the gingivae, with the common occurrence of bleeding but not discomfort[26]. The disease progresses

through 3 different phases, starting with the initial lesion; this forms within 4 days of plaque buildup and is accompanied with an acute inflammatory response though it is not clinically apparent[26]. After 7 days, the early lesion presents with now clinical levels of inflammation and a dense influx of lymphocytes; the presence of macrophages and plasma cells is also noted[26]. The lesion is finally referred to as an established lesion when predominantly anaerobic bacteria flourish, a periodontal pocket has formed, and there is a large population of plasma cells, B lymphocytes, and neutrophils[26]. While individuals can remain in this state for up to 10 years, without treatment the progression to periodontitis is possible[26]. It is therefore important to keep the gums healthy and plaque-free through proper oral hygiene to prevent the presentation of gingivitis.

3.1.2 DETECTION OF GINGIVAL INFLAMMATION USING OCT

While OCT has been extensively implemented for hard dental tissue assessment, its significance in the detection of gum-related problems remains quite uninvestigated. Researchers have explored the use of OCT in identifying gingival phenotype and thickness for the assessing the severity of periodontal disease as an alternative to the invasive current standard of periodontal probing[46,47]. It was established that OCT can be used to quantitatively assess gingival phenotype and be able to distinguish attached and free gingiva without touching or damaging the tissue[46,47]. Furthermore, the degree of periodontal detachment can be determined with OCT as demonstrated through preliminary studies by Damodaran *et al.* where they have identified and measured the separation between gingival and tooth boundaries[48].

These research efforts have been focused on assessing later-stage periodontal disease, and while this is important in disease management, it would be valuable to identify early indicators of disease such as inflammation and gingivitis so that progression into irreversible damage can be prevented. *In vivo* spectral imaging conducted by Zakian *et al.* assessed gingival inflammation by evaluating blood concentration and oxygenation through multispectral imaging at different wavelengths to determine the diffuse reflectance of the gingiva[49]. Absorption coefficients were extracted from this reflectance and inflammation was determined through spectral ratios, and they determined that their noninvasive imaging technique could distinguish between control and gingivitis-induced groups, with the spectral results correlating significantly with the clinical gingival index scores[49]. This method is limited in that it a reference measurement (pre-gingivitis) is needed, and is therefore confined to continual monitoring situations[49]. Detection of inflammation through OCT has been investigated in other tissues and pathologies, including the assessment of macrophage accumulation in atherosclerotic plaques; the increased presence of these inflammatory cells can be observed as a change in backscattered intensity of OCT images of the plaque[50]. It is therefore the hope of this thesis to be able to identify gingival inflammation through OCT-detectable differences caused by presence of inflammatory response cells and fluids.

3.2 HYPOTHESIS

The study described here aimed to establish whether *in vivo* optical coherence tomography (OCT) imaging could detect alterations in gingival tissue due to inflammation. Additional objectives of this secondary study were (i) to assess technical feasibility and

practical challenges of using OCT for intra-oral imaging, and (ii) to develop user-friendly image processing software for quantitative analysis of OCT images. The underlying hypotheses of the study were (i) that OCT imaging of the oral cavity can be performed *in vivo*, and (ii) that the gingival inflammation caused by brushing can be detected with OCT.

3.3 METHODS

For this chapter, I joined an ongoing pilot *in vivo* human gingival inflammation study, termed the 'parent study'. This parent study comprised 10 subjects and ran for two weeks (days 0 – 9), with OCT imaging performed on days 4 – 9. Baseline OCT images were taken prior to any treatment, and then subjects dry-brushed their teeth as a means of introducing inflammation in a controlled setting. Immediately after, post-treatment OCT scans were taken. Backscattered intensity as a function of depth was analyzed for both baseline and post-treatment scans, and the two were compared to determine if there was a significant change in OCT response post-brushing. For comparison, two parameters were extracted and compared: slope and area under the curve (AUC).

3.3.1 OCT HARDWARE

A Thorlabs Swept Source OCT System (Swept Source OCT OCS1300SS) and accompanying computer system unit, monitor, keyboard and mouse were set up for the OCT portion of the study. Note that the OCT images from this system use an inverted gray scale compared to the previous chapter (white = strong backscatter, black = weak backscatter). The system was connected according to the manual and optimized for clinical use. An external black-and-white camera (Point Grey Research Grasshopper3 GS3-

U3028S5M-C (Mono)) with a 25mm fixed focal length lens was secured and positioned as close as possible to the left of the OCT sample arm to provide the OCT-operator with real-time assistance in positioning the beam and confirming that the locations of the scan were correct. The camera software is displayed on one monitor while the OCT software runs on a second monitor. The setup is depicted in **Figure 24**.

Figure 24 – Clinical SS-OCT setup.

3.3.2 DATA ACQUISITION

To obtain data for analysis, the Thorlabs Swept Source OCT setup described in 3.3.1 and the Thorlabs Swept Source OCT Imaging System – Swept Source Optical Coherence Tomography Imaging System: Version 2.1.7 software were used to obtain OCT images of the subjects' gingival tissue. Subjects first underwent baseline OCT imaging prior to any treatment scheduled as part of the parent study. Each subject then dry brushed their teeth and immediately returned for post-treatment OCT imaging. In order to ensure

comparability of data, the OCT operator positioned the subject and the OCT camera so that the image was approximately divided into thirds: the left third would capture the labial side of the left central incisor, the middle third would capture the gingival tissues, and the right third would be the right central incisor (**Figure 25a**). A separate CCD camera provided a "live" image with the location of the scanning OCT beam visible (**Figure 25b**). This image was used to assist in the positioning of the OCT beam and confirm that the locations were correct. The distinct visibility of the dentin-enamel junction on OCT imaging was also utilized to as a guide to confirm which tissue was being imaged. For 5 out of the 6 days of the clinical trials, a single bitmap image was saved each for the baseline and post-treatment images. On the last day, a volume of 16 scans over 1 mm was taken for each subject.

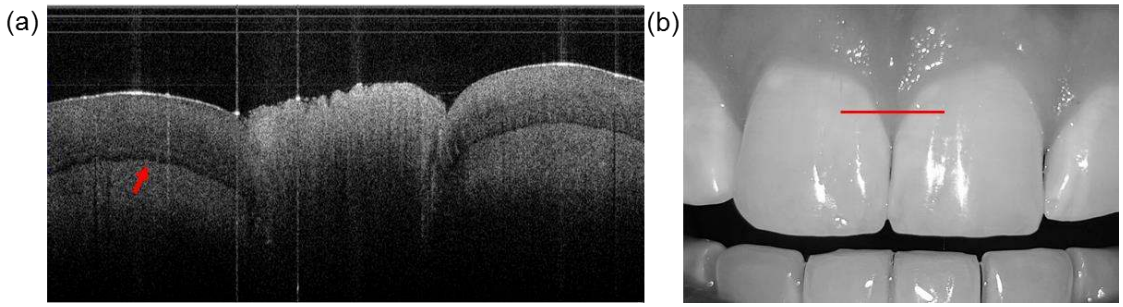

Figure 25 – **(a)** OCT image divided into thirds by left central incisor, gingival tissue, and the right central incisor. The distinct dentin-enamel junction (DEJ) is designated by the red arrow. **(b)** CCD camera image with scanning OCT beam indicated by the red line.

3.3.3 DATA ANALYSIS SOFTWARE AND PROCESSING

To determine whether or not the brushing procedure within the parent study had any OCT-detectable effect on the gingival tissue of the subjects, the backscattering intensity of the gingival tissue was assessed as a function of depth beneath the tissue surface. The gingiva can be separated into two components: the epithelium and the lamina

propria, which are both approximately 300 μm thick[51]. The lamina propria (connective tissue) contains blood vessels[52] and the inflammatory cells that travel through the junctional epithelium and into the gingival sulcus[53]. The hypothesis of this section was based on the possibility that brushing would induce an inflammatory response which may result in an alteration in the scattering or absorbing properties of the gingival tissue. This in turn may be detected as a reduced signal in OCT at the location of either of these tissue components, which will be apparent as either an alteration in the slope of the backscattered intensity vs depth plots or as a change in the area under these curves. Based on this hypothesis, the slopes of the intensity vs depth plots, and the area under the curve (AUC) of regions corresponding to each of the epithelium and the lamina propria were assessed.

The surface of the gingival tissue has a unique topography for each individual subject and can vary with location within each subject. To compensate for this, the surface of the tissue was detected using the MATLAB canny edge detection function (**Figure 26a**). Canny edge detection first eliminates noise by smoothing the image through Gaussian convolution. Then hysteresis thresholding is implemented with upper and lower thresholds. A pixel is accepted as an edge if its gradient is greater the upper threshold and it is rejected if it is below the lower threshold. When the gradient falls between the two values, the pixel will be accepted if it is connected to a pixel above the upper threshold, otherwise it will be excluded. The detected surface was then realigned to the top of the image, providing an even surface from which the intensity versus depth profile of the tissue can be analyzed, independent of lateral location (**Figure 26b**).

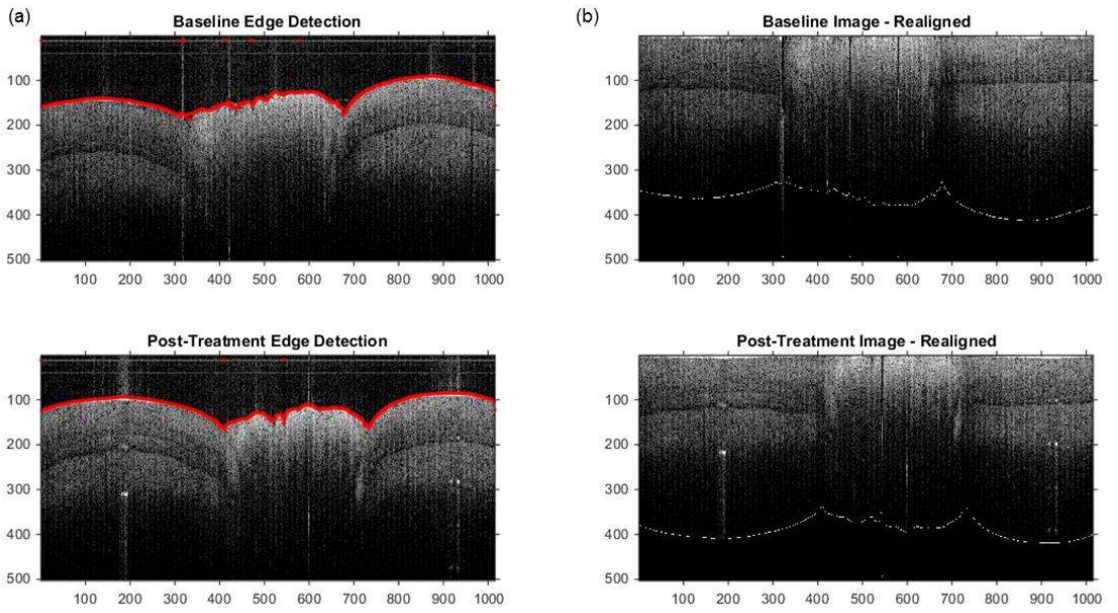

Figure 26 – **(a)** Canny edge detection results for baseline and post-treatment OCT images. **(b)** Realignment of tissue surface to the top of the image for both baseline and post-treatment OCT images.

Prior to analyzing the OCT backscattered intensity versus depth profile, accurate identification of the tissue surface was established by selection of an appropriate threshold for the edge detection algorithm. A Matlab m-file (TestEdgeDetection.m) was created to display the edge detection results of four different thresholds on the same image. The range which provided the most accurate detection of the gingival tissue surface was logged in a .txt file for later use. This process was repeated for each OCT image, (baseline and post-treatment), for each subject, on each trial date.

The edge detection thresholds along with the dates of the trials that each subject participated in were entered into a separate Matlab script. This script looped through each trial date and displayed the baseline and post-treatment images of the central incisors and gingiva together for comparison, one trial date at a time. These images displayed the detected surface of the gingival tissue as a red overlay. The region of gingival tissue was

then selected by clicking the left and right gingival margins for the baseline image, and then again for the post-treatment image. Once these four points were selected, the program generated an image displaying these selections on the surface-realigned images for review by the user (**Figure 27a**). The mean OCT backscattered intensity versus depth profile was then generated by calculating the average backscattered signal at each depth pixel for this selection of gingival tissue, displaying the baseline and post-treatment profiles on the same figure in different colors for comparison (**Figure 27b**).

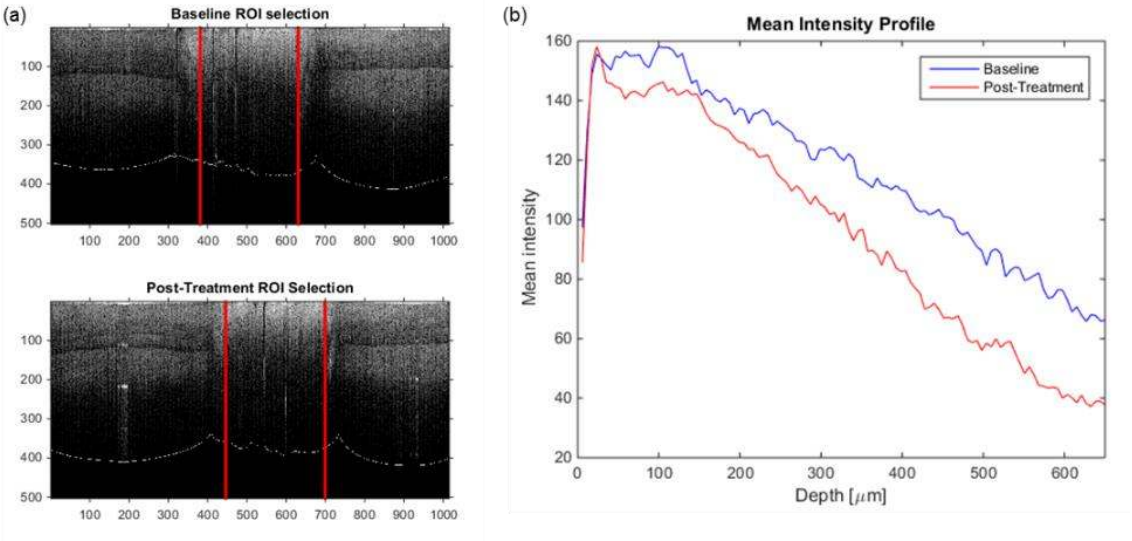

Figure 27 – **(a)** The user-selected ROI's (within the red vertical lines) for baseline and post-treatment OCT images. **(b)** Mean backscattered intensity profile as a function of depth comparing the baseline and post-treatment results.

As a result of the close proximity of the OCT camera unit to the subjects, there was an overall dimming effect due to "fogging" on some of the OCT images. "Fogging" refers to the development of condensation on the OCT camera lens due to the subject breathing on this glass surface. Condensation on the lens results in a uniform attenuation of the OCT beam to and from the subject, with a consequent reduction in the measured intensity.

During imaging sessions, this effect was minimized by pausing between measurements to allow the condensation to clear. To compensate for any residual effect on the quantitative results, the baseline and post-treatment intensity vs depth plots were corrected such that the tissue surface peaks became aligned to each other. This was accomplished by vertically shifting all data points in the post-treatment profile by an amount required to bring the tissue surface peak to the same intensity level as the baseline peak. This correction method was validated with a separate experiment in which a uniform phantom was first imaged using OCT, and then an attenuator was applied to mimic the attenuation due to fogging and the sample was imaged again. If peak alignment is a valid method, then realignment of the plots should make them overlap almost perfectly, as was the case in our experiment (**Figure 28**).

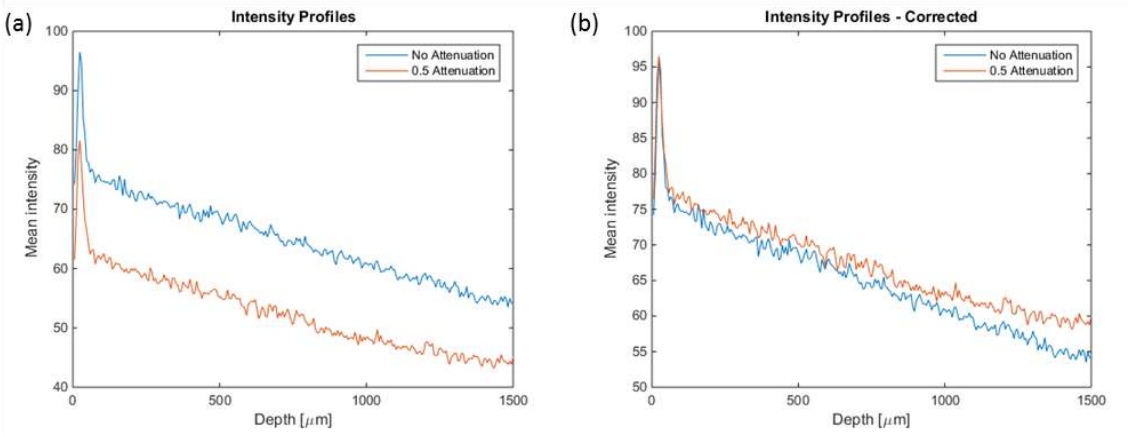

Figure 28 – **(a)** Mean backscattered intensity versus depth plot for phantom, showing attenuator effect. **(b)** Mean backscattered intensity versus depth plots for phantom corrected through peak alignment and subsequent adjustment of the remaining values.

Linear least squares fits to the intensity vs depth plots were established separately for the epithelium and lamina propria regions (**Figure 29**). The area under the curve was

also determined for these regions and all data exported to an Excel file for further statistical analysis.

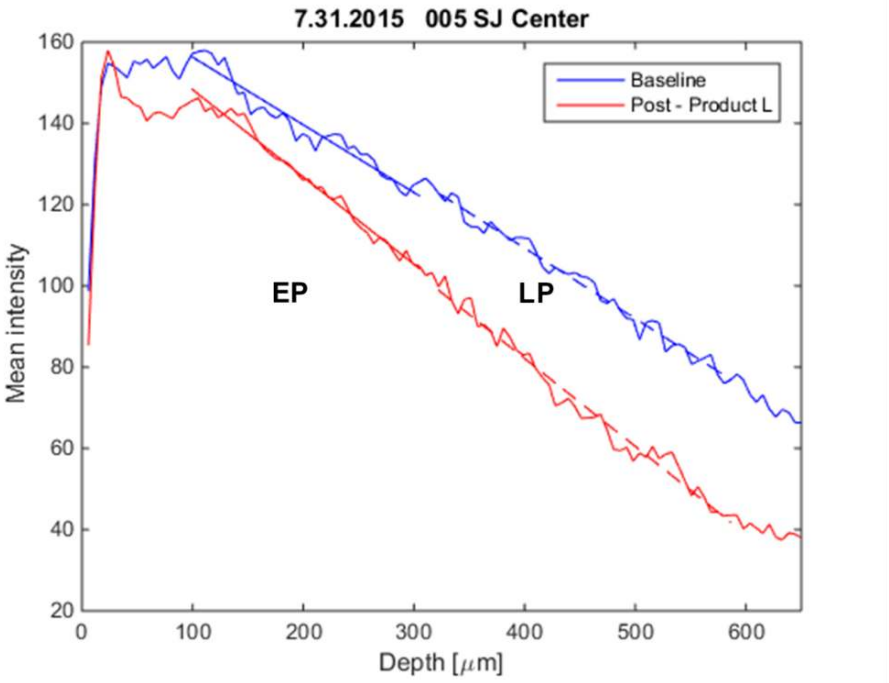

Figure 29 – Mean backscattered intensity versus depth plot for subject 5, comparing baseline and post-treatment results. Epithelium (EP) and Lamina Propria (LP) regions are indicated on the plots, and a linear fit is provided for each region.

3.3.4 CREATION OF MATLAB GRAPHICAL USER INTERFACES

Clinical trials require fast and efficient processing of large amounts of data. To provide this, three MATLAB graphical user interfaces (GUIs) were created. The first program (**Figure 30**) generates a folder based on the subject and trial details loaded by the user. After entering in the file names of the saved volume scans (.IMG format), the program will display the baseline and post treatment volumes side-by-side for easy comparison. The user can the scroll through each scan to find a pair that match best in

location. Once satisfied, the selection can be confirmed and these two images will be saved as bitmaps in the previously created folder.

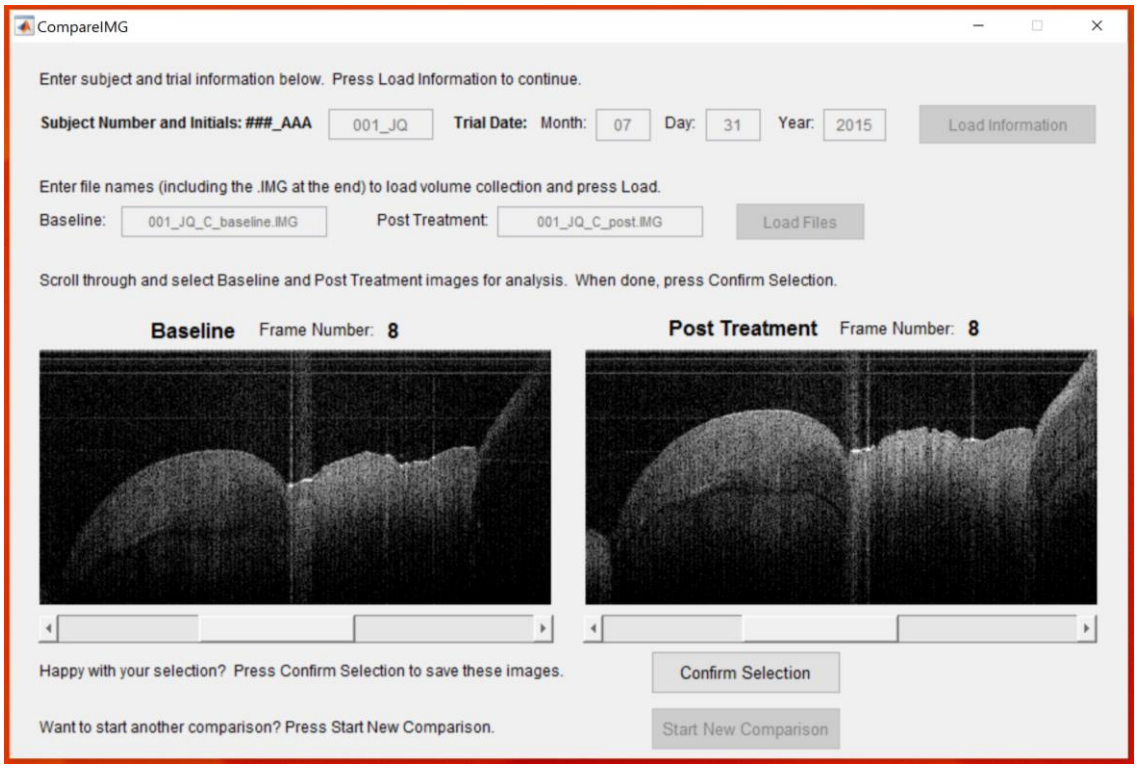

Figure 30 – MATLAB GUI for manual side-by-side comparisons of baseline and post-treatment OCT scans.

Due to fogging and experimental factors, the intensity of the tissue surface varies between images, so the Canny threshold values have to be tailored for each one. To do this easily, the next program allows the user to load the previously selected baseline and post treatment images (**Figure 31**). It then allows the user to enter in lower and upper thresholds for each image and see how well they detect the surface of the gingiva; a red line will illustrate what edge is detected with the chosen threshold values. From experience, there were several combinations that worked well for most of the images analyzed for the clinical

study, so these are provided to give the user an idea of what works and how to adjust it accordingly. Once the ideal threshold values are determined, the user can then save these values to be used for the final analysis.

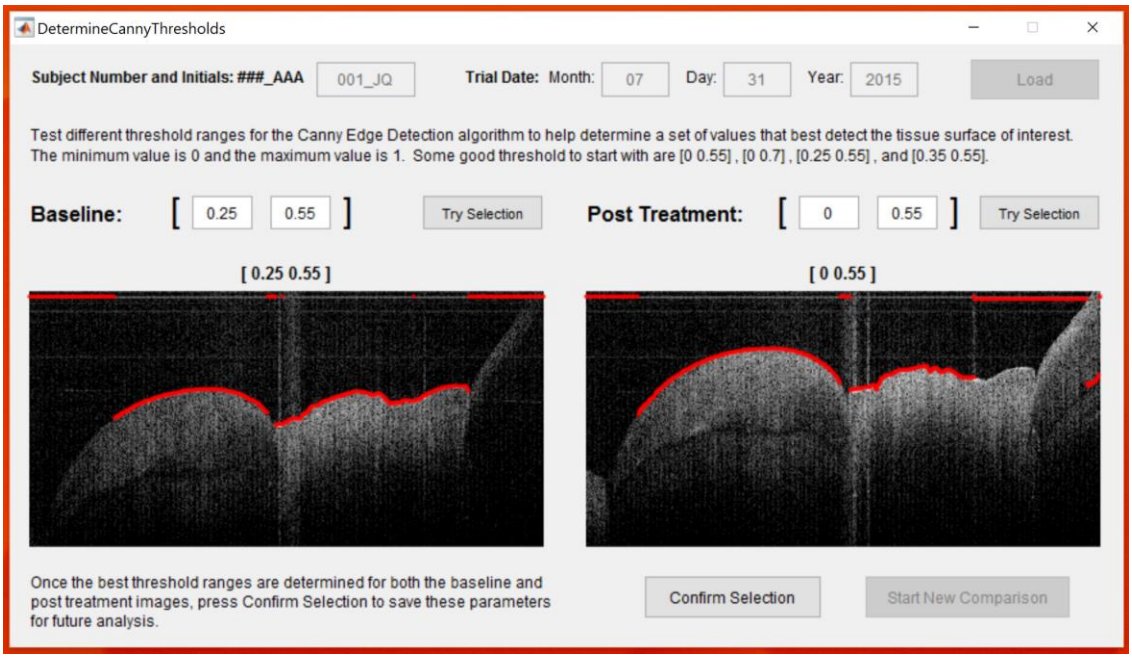

Figure 31 – MATLAB GUI for manual determination of appropriate Canny edge detection threshold values for each set of baseline and post-treatment OCT scans.

The last program created completes the analysis of the images (**Figure 32**). After the subject and trial information is loaded, the images are displayed for viewing. Once the Continue Analysis button is pressed, the edge detection is displayed and a selection tool is provided.

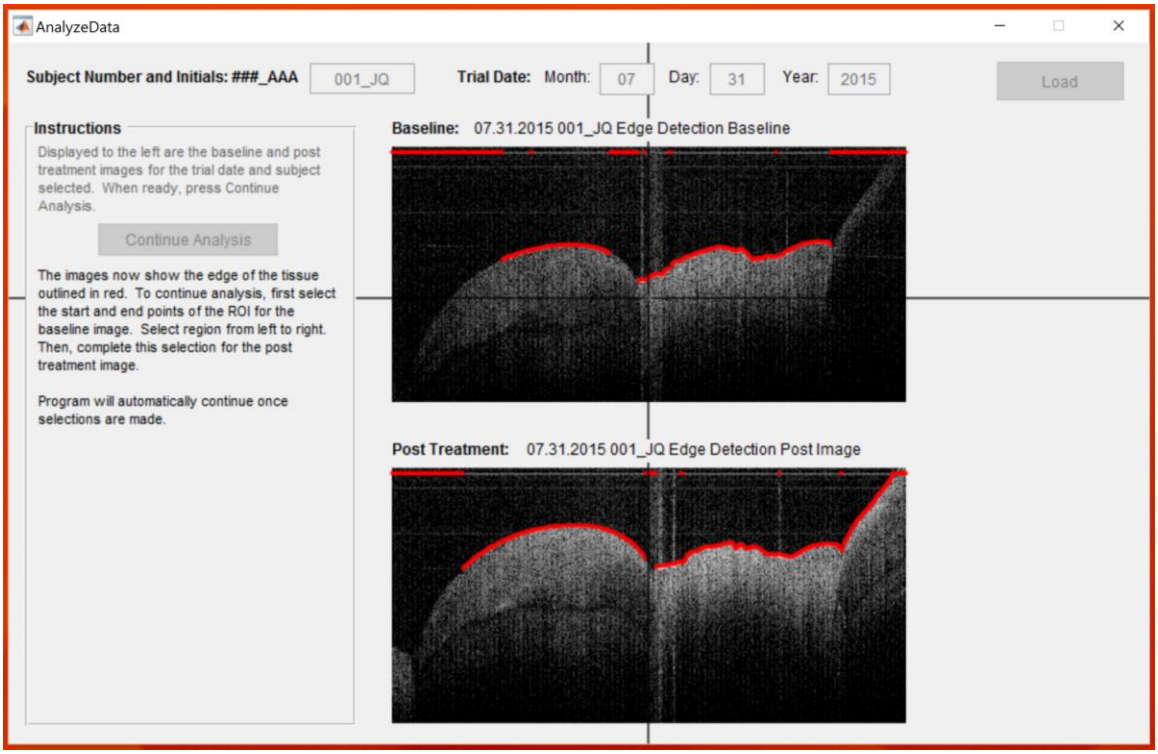

Figure 32 – MATLAB GUI for manual selection of region-of-interest for baseline and post-treatment options.

The user then selects the region of interest from left to right on the baseline image, and repeats this for the post treatment image. After these four points are selected, the program will automatically generate the mean intensity profile, and the user can then select the region of interest from left to right for further analysis (**Figure 33**).

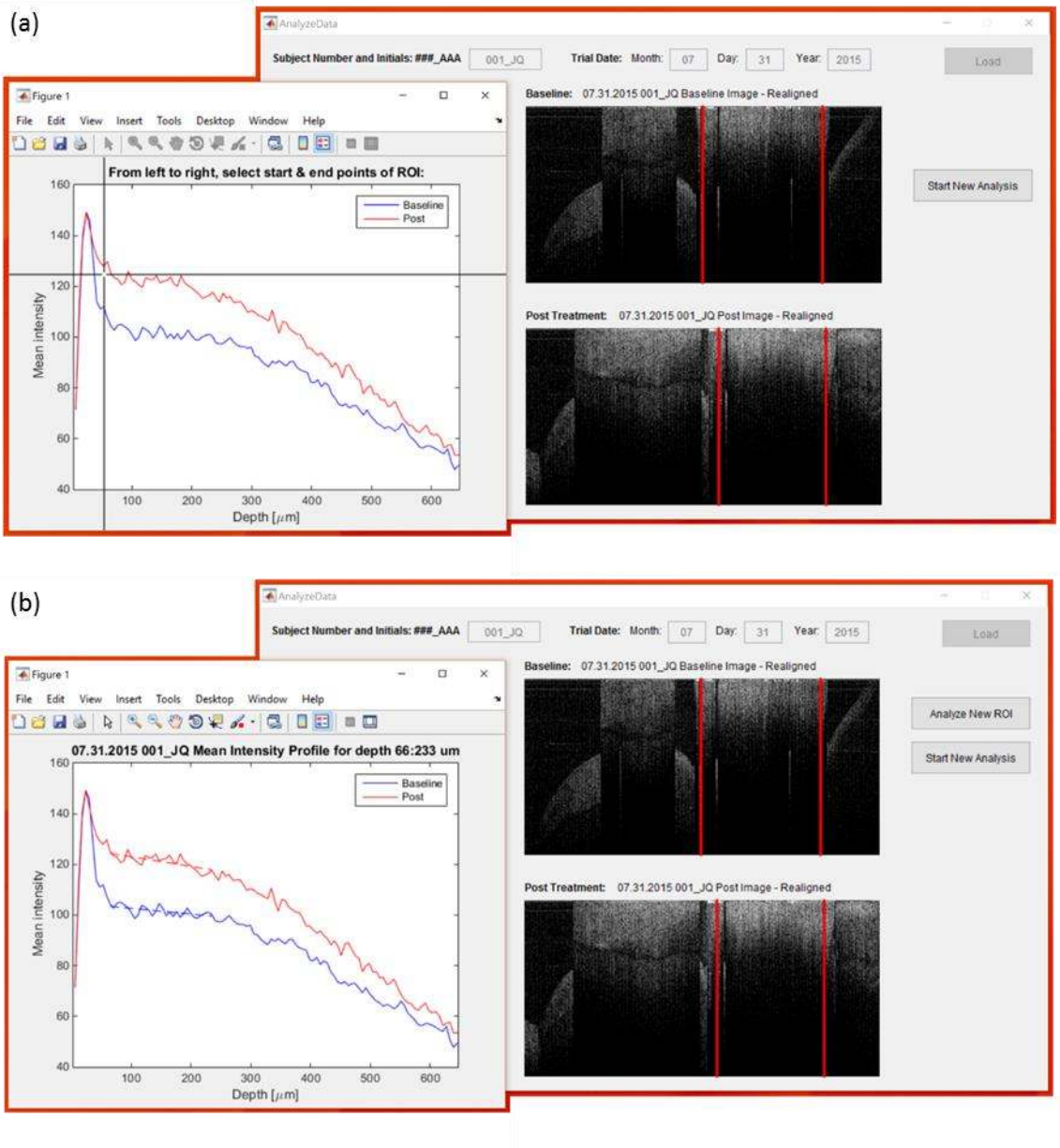

Figure 33 – **(a)** User selects, from left to right, the region-of-interest for further analysis. **(b)** Once the selection is made, the program generates a mean backscattered intensity versus depth profile for this baseline and post-treatment set, and important values are written to an Excel sheet automatically.

After the selection has been made, line of best fit of the region of interest is displayed and slope and AUC values for this depth selection are exported to an Excel file specific to the subject. If another region on the same plot is desired, the user can press the

Analyze New ROI button and the mean intensity profile plot will show again with the select tool; the new values generated will be saved to the same Excel file, keeping all of the subject's data together. These GUIs allow for quick and organized results. There also exists the potential for an automated region selection of A-lines for averaging depending on the tissue of interest. The program could select the area of interest using different landmarks within the image (such as the DEJ) as guides, and this could make the analysis easier and also more consistent.

3.4 RESULTS

Due to the late inclusion of this secondary project onto the parent study, OCT data was collected for just one day (day 4) of week 1. While there were 5 days of OCT data acquisition for week 2, on average each subject had about 3 useable days. This was a result of suboptimal matching of baseline and post-treatment imaging locations. The factor change (FC) between post-treatment and baseline was calculated for the slope and AUC parameters. Comparisons of baseline and post-treatment in terms of these FC calculations are provided for the epithelium (**Figure 34**) and for the lamina propria (**Figure 35**). An FC of one indicates no difference between post and baseline; an FC less than one indicates a decrease in value post-treatment; an FC greater than one indicates an increase in value post-treatment.

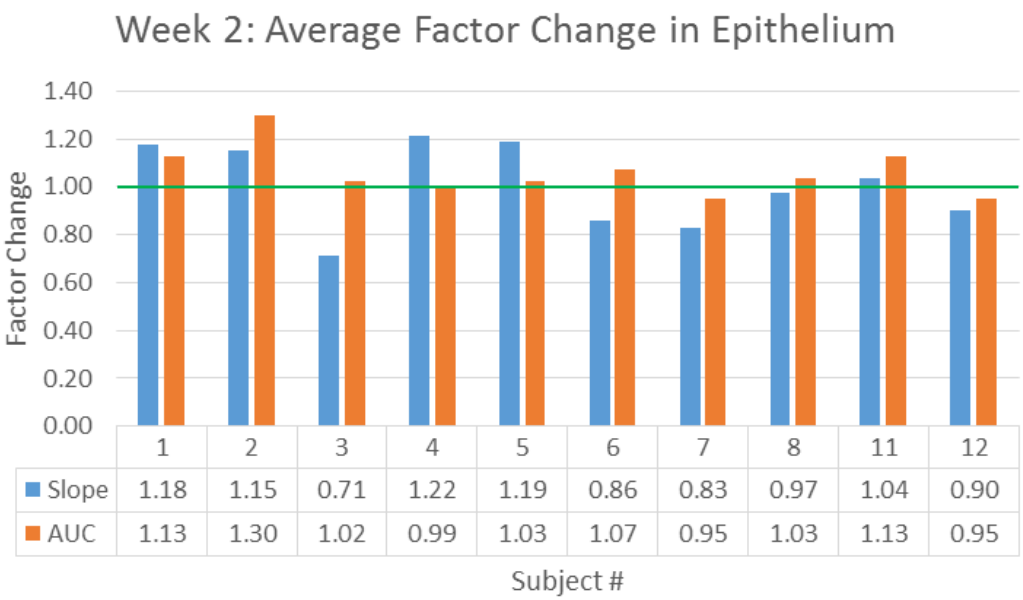

Figure 34 – Factor change for slope and area-under-the-curve (AUC) for the epithelium. A factor change of 1 (no change) is indicated by the green line for reference.

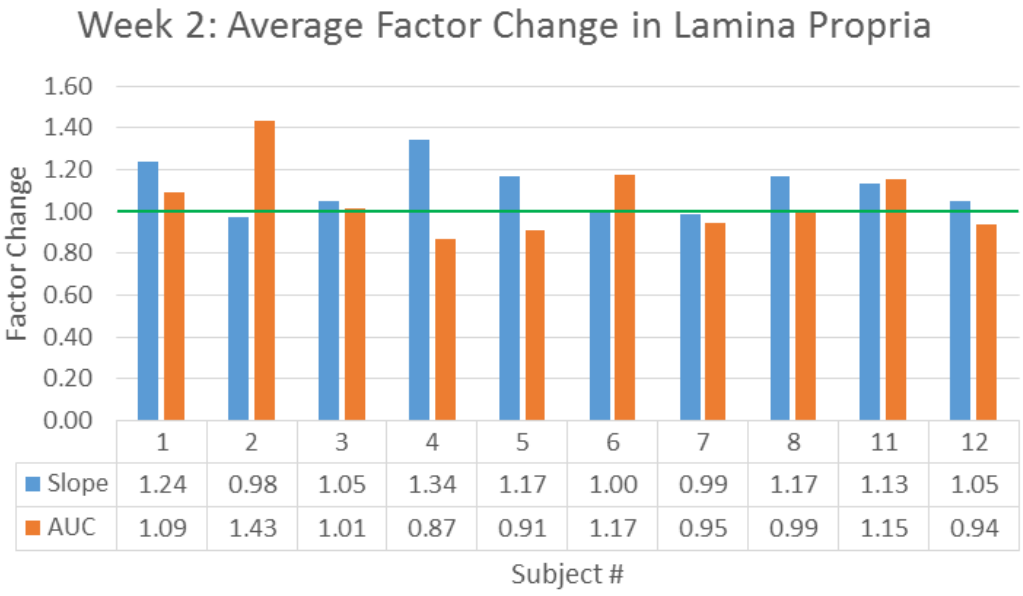

Figure 35 – Factor change for slope and area-under-the-curve (AUC) for the lamina propria. A factor change of 1 (no change) is indicated by the green line for reference.

With the null hypothesis being that there is no change induced post-brushing (FC = 1), a t-test was performed to determine the probability of this sample population having such a factor change. Each parameter was averaged across the ten subjects and the standard deviation calculated; using Excel, the t-test was performed and *p*-values determined for slope and AUC for both the epithelium and lamina propria. These calculations indicated no appreciable factor change in either slope or AUC for the epithelium ($p > 0.05$) and no appreciable factor change in the AUC for the lamina propria ($p > 0.05$). There was a significant factor change in slope for the lamina propria region ($p < 0.05$). This is visualized in **Figure 36**.

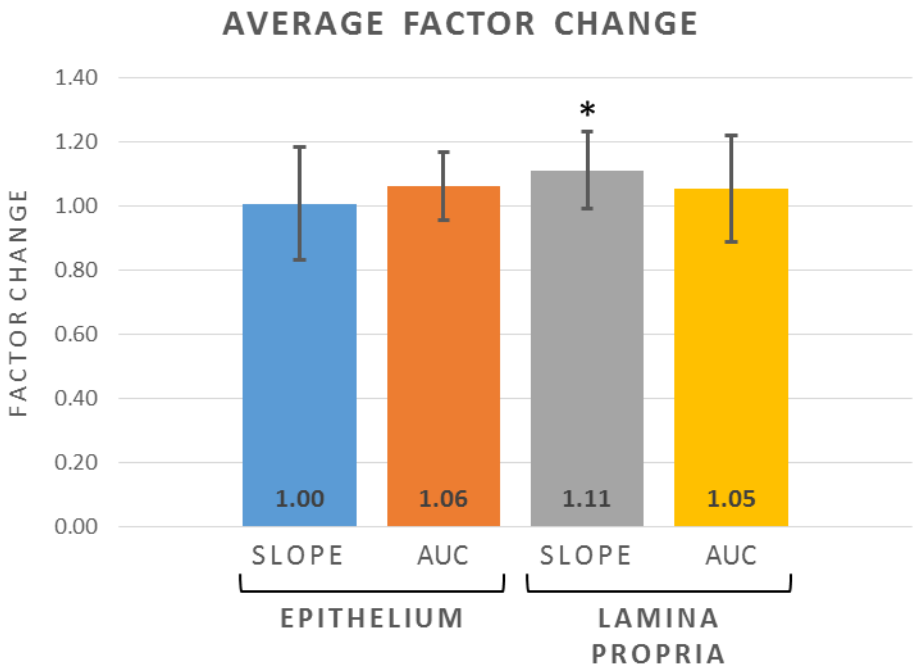

Figure 36 – Average factor change for slope and area-under-the-curve (AUC) for the epithelium and the lamina propria. The statistically significant factor change in lamina propria slope is indicated with an asterisk.

3.5 DISCUSSION & CONCLUSIONS

This trial was valuable for establishing reproducible and reliable methods for both intra-oral OCT data acquisition and analysis. The addition of the external camera provided desired visual guidance and allowed for more accurate image acquisition. The acquired 2D bitmap images were successfully manipulated and analyzed using MATLAB, and important quantitative information was obtained and outputted. This code was further developed into a user-friendly and interactive processing software that allows the operator to select the appropriate parameters specific to the study. The program keeps the files well organized, exporting and saving all figures, variables, and values into a subject-labeled folder.

From this study, I cannot conclude that the brushing had an appreciable effect on the measured OCT backscatter signal. There was a significant factor change in the slope of OCT signal in the lamina propria region of the gingiva, and while this may not be enough to make firm conclusions on the capability of OCT in detecting inflammation, it provides motivation to investigate this modality further with some experimental adjustments. OCT was originally not included in the parent study, and our late entry into the trial only allowed for us to acquire data for one day of the first week; while I took images for all days of week 2, some of the baseline and post-treatment images were not comparable in location and were therefore not used for analysis. It is possible that there may be an OCT-detectable difference in gingival backscatter and (1) there simply was not enough data to show this, or (2) the brushing method did not induce significant amounts of inflammation to be detected with OCT.

OCT can collect 3D data, saving many 2D images over a specified volume. Due to the late addition of this secondary study to the parent study, I was not able to fully utilize this feature for the current study. I did, however, established code and user-friendly software that extracts the separate images from the volume data and displays the baseline and post-treatment collections side-by-side for ease of comparison. The user can then select which baseline and post-treatment pair are most similar and save these 2D images for analysis. Proper data acquisition is critical for obtaining comparable results, and from this study methods were established to ensure the usability of the attained images and have created software to analyze the results in a way that can be tailored to the aim of the study.

CHAPTER 4: DISCUSSION

4.1 SUMMARY OF RESULTS

The demineralization *in vitro* chapter allowed for several conclusions, with the first being the confirmation of my hypothesis that changes in OCT signal are directly correlated with microhardness changes. I was also able to establish that the diluted phosphoric acid solution produced a time-dependent demineralization response and that OCT can successfully distinguish this trend. This correlation and the understanding of how the OCT setup identifies demineralization allows for confident progression of experimentation into *in vivo* studies.

The *in vivo* gingival study revealed that there is a significant factor change in slope of the lamina propria region of the gingiva after the brushing procedure. This suggests that OCT may be able to detect inflammation and provides motivation for further investigation. Efficient, user-friendly programs have been created to facilitate data analysis and provide dependable and organized results. The appropriate adjustments were made to improve data acquisition, such as the inclusion of a camera for improved probe alignment and an algorithm to correct for dimmed signal due to fogging. This study showcased the feasibility of using OCT in a clinical setting as a quick and non-invasive method for detecting dental issues.

4.2 FUTURE WORK

With these preliminary studies completed, there are a few more steps that need to be completed before transitioning this technology into the clinical setting. While a dose-dependent enamel demineralization response was observed with 30% H_3PO_4 within a 5

second exposure time, these conditions likely produce a more rapid and aggressive etch than will be encountered *in vivo*. Future work includes adjusting the enamel exposure conditions to produce a milder etch, in order to achieve a more gradual dose response and to provide a more appropriate *in vivo* solution and demineralization response. This could be achieved either through greater dilution of the phosphoric acid or by using a different mildly acidic solution, such as soda or orange juice. Further *in vitro* testing must be completed to determine whether OCT can quantify demineralization (a) under conditions that can be applied in *in vivo* studies, and (b) under exposure to everyday levels of demineralizing drinks.

For the gingival study, although the results show some indication that OCT may be a valuable diagnostic tool for assessment of inflammation, it is unclear exactly how much inflammation was induced with the simple brushing exercise. In order to assess whether clinically relevant inflammation levels affect OCT signals, it would be useful to measure the OCT response in individuals with clinical presentation of gingivitis. This would allow for the establishment of which subsurface tissue region (epithelium, lamina propria or the whole gingival depth) and which OCT criteria (slope, area under the curve, or other) should be used to assess inflammation in the future when it is induced experimentally. When inflammation is induced experimentally with brushing, it would also be valuable to have a control, no brushing region to determine the natural fluctuations in gingival signal.

The long term goal of this research is to establish OCT as a noninvasive tool for the assessment and diagnosis of early dental diseases, including enamel demineralization and gingivitis. While the current commercially available Thorlabs setup was adequate for imaging the gingiva in the front of the mouth, a handheld probe will be needed for gaining

access to the inner gums and molars. Such a probe has been created by other researchers in the lab and is pictured below (**Figure 37**).

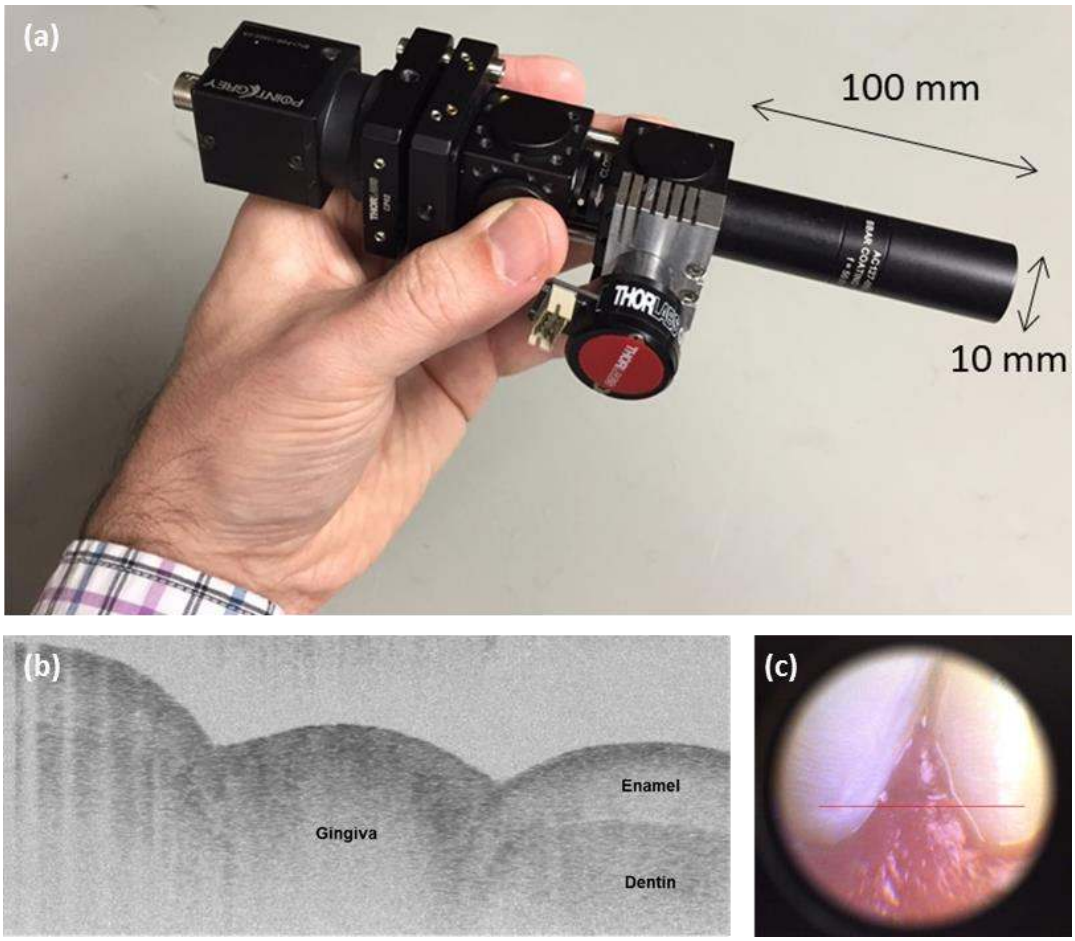

Figure 37 – **(a)** Image of the handheld OCT probe. **(b)** An example of an OCT scan of the bottom incisors with gingiva in between. **(c)** CCD view from back of the handheld probe, with OCT beam indicated by the red line.

The use of such a handheld device could allow for viewing of hard to reach areas and could also prevent the fogging issue seen with the stationary setup since it can be held flush against the tissue and will not be contact with the subject's warm breath. Various probe attachments can be 3D printed to allow for the probe to access different areas within the mouth. An attachment similar to that presented in **Figure 35** is appropriate for imaging

tissue in the front of the mouth. Additionally, an attachment with a tip that is bent 90^{o} downwards can allow for access to top and sides of back molars. This probe therefore permits an easy transition from *in vitro* to *in vivo* work.

4.3 SUMMARY AND CONCLUSION

In this thesis, OCT was investigated for quantitative assessment of hard and soft oral tissues in *in vitro* and *in vivo* studies. The enamel demineralization study established a preliminary relationship between non-destructive OCT measurement and a current (destructive) gold-standard of microhardness testing; this allowed for confident conclusions regarding demineralization responses. The strength of the phosphoric acid used proved to be a limitation of this study since in provided too strong and quick of a response for *in vivo* translation. Future work focused on adjusting the demineralization solution can overcome this issue and push this *in vitro* work into clinical studies.

The gingival study led to the development of the necessary protocols and software to perform *in vivo* measurements in future studies. A limitation of this work is that there was no independent methodology used to determine whether or not the brushing procedure induced a definitive inflammatory reaction, or what grade of inflammation was induced. This limitation can be amended in the future by either first imaging subjects with significant clinical gingivitis to determine the OCT response to inflammation, or by introducing another technique such as checking salivary biomarkers[3,4] in order to establish that there is in fact inflammation present. Together, these *in vitro* and *in vivo* research efforts suggest that OCT imaging may be an effective tool for longitudinal monitoring of hard and soft tissue conditions in the human oral cavity.

CHAPTER 5: REFERENCES

1. Garcia RI, Henshaw MM, Krall EA. Relationship between periodontal disease and systemic health. *Periodontology 2000.* 2001;25(1):21-36.
2. Hale KJ. Oral health risk assessment timing and establishment of the dental home. *Pediatrics.* 2003;111(5 Pt 1):1113-1116.
3. Giannobile WV, Beikler T, Kinney JS, Ramseier CA, Morelli T, Wong DT. Saliva as a diagnostic tool for periodontal disease: current state and future directions. *Periodontology 2000.* 2009;50(1):52-64.
4. Armitage GC. The complete periodontal examination. *Periodontology 2000.* 2004;34(1):22-33.
5. Shimada Y, Sadr A, Sumi Y, Tagami J. Application of Optical Coherence Tomography (OCT) for Diagnosis of Caries, Cracks, and Defects of Restorations. *Current Oral Health Reports.* 2015;2(2):73-80.
6. Huang D, Swanson EA, Lin CP, et al. Optical coherence tomography. *Science.* 1991;254(5035):1178-1181.
7. Fujimoto JG, Pitris C, Boppart SA, Brezinski ME. Optical coherence tomography: an emerging technology for biomedical imaging and optical biopsy. *Neoplasia.* 2000;2(1):9-25.
8. Chen TC, Cense B, Pierce MC, et al. Spectral domain optical coherence tomography: ultra-high speed, ultra-high resolution ophthalmic imaging. *Archives of ophthalmology.* 2005;123(12):1715-1720.
9. Bouma BE, Yun S-H, Vakoc BJ, Suter MJ, Tearney GJ. Fourier-domain optical coherence tomography: recent advances toward clinical utility. *Current opinion in biotechnology.* 2009;20(1):111-118.
10. Choma M, Sarunic M, Yang C, Izatt J. Sensitivity advantage of swept source and Fourier domain optical coherence tomography. *Optics express.* 2003;11(18):2183-2189.
11. Fercher AF, Hitzenberger CK, Kamp G, El-Zaiat SY. Measurement of intraocular distances by backscattering spectral interferometry. *Optics Communications.* 1995;117(1):43-48.
12. Fercher AF. Optical coherence tomography. *Journal of Biomedical Optics.* 1996;1(2):157-173.
13. Wojtkowski M, Srinivasan V, Ko T, Fujimoto J, Kowalczyk A, Duker J. Ultrahigh-resolution, high-speed, Fourier domain optical coherence tomography and methods for dispersion compensation. *Optics express.* 2004;12(11):2404-2422.
14. Adhi M, Duker JS. Optical coherence tomography–current and future applications. *Current opinion in ophthalmology.* 2013;24(3):213.
15. Tearney GJ, Regar E, Akasaka T, et al. Consensus standards for acquisition, measurement, and reporting of intravascular optical coherence tomography studies: a report from the International Working Group for Intravascular Optical Coherence Tomography Standardization and Validation. *Journal of the American College of Cardiology.* 2012;59(12):1058-1072.

16. Suter MJ, Gora MJ, Lauwers GY, et al. Esophageal-guided biopsy with volumetric laser endomicroscopy and laser cautery marking: a pilot clinical study. *Gastrointestinal endoscopy.* 2014;79(6):886-896.
17. Colston BW, Everett MJ, Da Silva LB, Otis LL, Stroeve P, Nathel H. Imaging of hard-and soft-tissue structure in the oral cavity by optical coherence tomography. *Applied Optics.* 1998;37(16):3582-3585.
18. Baumgartner A, Dichtl S, Hitzenberger C, et al. Polarization–sensitive optical coherence tomography of dental structures. *Caries research.* 2000;34(1):59-69.
19. Jones RS, Darling CL, Featherstone JD, Fried D. Remineralization of in vitro dental caries assessed with polarization-sensitive optical coherence tomography. *Journal of biomedical optics.* 2006;11(1):014016-014016-014019.
20. De Boer JF, Milner TE, van Gemert MJ, Nelson JS. Two-dimensional birefringence imaging in biological tissue by polarization-sensitive optical coherence tomography. *Optics letters.* 1997;22(12):934-936.
21. Hitzenberger C, Götzinger E, Sticker M, Pircher M, Fercher A. Measurement and imaging of birefringence and optic axis orientation by phase resolved polarization sensitive optical coherence tomography. *Optics Express.* 2001;9(13):780-790.
22. Fried D, Xie J, Shafi S, Featherstone JD, Breunig TM, Le C. Imaging caries lesions and lesion progression with polarization sensitive optical coherence tomography. *Journal of biomedical optics.* 2002;7(4):618-627.
23. Jones RS, Staninec M, Fried D. Imaging artificial caries under composite sealants and restorations. *Journal of Biomedical Optics.* 2004;9(6):1297-1304.
24. Shimada Y, Nakagawa H, Sadr A, et al. Noninvasive cross-sectional imaging of proximal caries using swept-source optical coherence tomography (SS-OCT) in vivo. *Journal of biophotonics.* 2014;7(7):506-513.
25. Lenton P, Rudney J, Chen R, Fok A, Aparicio C, Jones RS. Imaging in vivo secondary caries and ex vivo dental biofilms using cross-polarization optical coherence tomography. *Dental materials.* 2012;28(7):792-800.
26. Samaranayake LP. *Essential microbiology for dentistry.* Elsevier Health Sciences; 2006.
27. Robinson C, Shore R, Brookes S, Strafford S, Wood S, Kirkham J. The chemistry of enamel caries. *Critical Reviews in Oral Biology & Medicine.* 2000;11(4):481-495.
28. Yanagisawa T, Miake Y. High-resolution electron microscopy of enamel-crystal demineralization and remineralization in carious lesions. *Journal of electron microscopy.* 2003;52(6):605-613.
29. Hsu DJ, Darling CL, Lachica MM, Fried D. Nondestructive assessment of the inhibition of enamel demineralization by CO2 laser treatment using polarization sensitive optical coherence tomography. *Journal of biomedical optics.* 2008;13(5):054027-054027-054029.
30. Popescu DP, Sowa MG, Hewko MD. Assessment of early demineralization in teeth using the signal attenuation in optical coherence tomography images. *Journal of biomedical optics.* 2008;13(5):054053-054053-054058.
31. Kang H, Jiao JJ, Lee C, Le MH, Darling CL, Fried D. Nondestructive assessment of early tooth demineralization using cross-polarization optical coherence

tomography. *Selected Topics in Quantum Electronics, IEEE Journal of.* 2010;16(4):870-876.
32. Shimada Y, Sadr A, Burrow MF, Tagami J, Ozawa N, Sumi Y. Validation of swept-source optical coherence tomography (SS-OCT) for the diagnosis of occlusal caries. *Journal of Dentistry.* 2010;38(8):655-665.
33. Chan KH, Chan AC, Darling CL, Fried D. Methods for monitoring erosion using optical coherence tomography. Paper presented at: SPIE BiOS2013.
34. Lee RC, Darling CL, Fried D. Automated detection of remineralization in simulated enamel lesions with PS-OCT. Paper presented at: SPIE BiOS2014.
35. Mandurah MM, Sadr A, Shimada Y, et al. Monitoring remineralization of enamel subsurface lesions by optical coherence tomography. *Journal of biomedical optics.* 2013;18(4):046006-046006.
36. Sadr A, Mandurah M, Nakashima S, et al. Monitoring of enamel lesion remineralization by optical coherence tomography: an alternative approach towards signal analysis. Paper presented at: SPIE BiOS2013.
37. Chew H, Zakian C, Pretty I, Ellwood R. Measuring initial enamel erosion with quantitative light-induced fluorescence and optical coherence tomography: an in vitro validation study. *Caries research.* 2014;48(3):254-262.
38. Nakajima Y, Shimada Y, Sadr A, et al. Detection of occlusal caries in primary teeth using swept source optical coherence tomography. *Journal of biomedical optics.* 2014;19(1):016020-016020.
39. Chan KH, Chan AC, Fried WA, Simon JC, Darling CL, Fried D. Use of 2D images of depth and integrated reflectivity to represent the severity of demineralization in cross-polarization optical coherence tomography. *Journal of biophotonics.* 2015;8(1-2):36-45.
40. Fried D, Staninec M, Darling CL, Chan KH, Pelzner RB. Clinical monitoring of early caries lesions using cross polarization optical coherence tomography. Paper presented at: Proc. of SPIE Vol2013.
41. Nee A, Chan K, Kang H, Staninec M, Darling CL, Fried D. Longitudinal monitoring of demineralization peripheral to orthodontic brackets using cross polarization optical coherence tomography. *Journal of dentistry.* 2014;42(5):547-555.
42. Ibusuki T, Kitasako Y, Sadr A, Shimada Y, Sumi Y, Tagami J. Observation of white spot lesions using swept source optical coherence tomography (SS-OCT): in vitro and in vivo study. *Dental materials journal.* 2015;34(4):545-552.
43. Takamizawa T, Barkmeier W, Tsujimoto A, et al. Effect of phosphoric acid pre-etching on fatigue limits of self-etching adhesives. *Operative dentistry.* 2015;40(4):379-395.
44. West N, Hughes J, Addy M. Erosion of dentine and enamel in vitro by dietary acids: the effect of temperature, acid character, concentration and exposure time. *Journal of oral rehabilitation.* 2000;27(10):875-880.
45. Louie T, Lee C, Hsu D, et al. Clinical assessment of early tooth demineralization using polarization sensitive optical coherence tomography. *Lasers in surgery and medicine.* 2010;42(10):898-905.
46. Mota CC, Fernandes LO, Melo LS, Feitosa DS, Cimões R, Gomes AS. Comparative analysis of gingival phenotype in animal and human experimental

models using optical coherence tomography in a non-invasive approach. Paper presented at: SPIE Biophotonics South America2015.
47. Mota CC, Fernandes LO, Cimoes R, Gomes AS. Non-Invasive Periodontal Probing Through Fourier-Domain Optical Coherence Tomography. *Journal of periodontology.* 2015;86(9):1087-1094.
48. Damodaran V, Vasa NJ, Sarathi R, Rao SR. Non-invasive detection of periodontal loss of attachment using optical coherence tomography. Paper presented at: International Conference on Optics & Photonics 20152015.
49. Zakian C, Pretty I, Ellwood R, Hamlin D. In vivo quantification of gingival inflammation using spectral imaging. *Journal of biomedical optics.* 2008;13(5):054045-054045-054049.
50. Tearney GJ, Yabushita H, Houser SL, et al. Quantification of macrophage content in atherosclerotic plaques by optical coherence tomography. *Circulation.* 2003;107(1):113-119.
51. Feldchtein F, Gelikonov V, Iksanov R, et al. In vivo OCT imaging of hard and soft tissue of the oral cavity. *Optics Express.* 1998;3(6):239-250.
52. Palumbo A. *The anatomy and physiology of the healthy periodontium.* INTECH Open Access Publisher; 2011.
53. Nanci A, Bosshardt DD. Structure of periodontal tissues in health and disease*. *Periodontology 2000.* 2006;40(1):11-28.